Cerebral Cortex November 2015;25:4076–4093
doi:10.1093/cercor/bhu122
Advance Access publication June 5, 2014

Functional Maturation of GABA Synapses During Postnatal Development of the Monkey Dorsolateral Prefrontal Cortex

Guillermo Gonzalez-Burgos[1], Takeaki Miyamae[1], Diego E. Pafundo[1,4], Hiroki Yoshino[1,5], Diana C. Rotaru[1,6], Gil Hoftman[1], Dibyadeep Datta[1], Yun Zhang[2], Mahjub Hammond[3], Allan R. Sampson[2], Kenneth N. Fish[1], G. Bard Ermentrout[3] and David A. Lewis[1]

[1]Translational Neuroscience Program, Department of Psychiatry, University of Pittsburgh School of Medicine, Pittsburgh, PA 15261, USA, [2]Department of Statistics, [3]Department of Mathematics, University of Pittsburgh, Pittsburgh, PA, USA, [4]Current address: Department of Biological Sciences, Carnegie Mellon University, Pittsburgh, USA, [5]Current address: Department of Psychiatry, Nara Medical University, Japan and [6]Current address: Department of Integrative Neurophysiology, Vrije Universiteit, Amsterdam, Netherlands

Address correspondence to Guillermo Gonzalez-Burgos, David A. Lewis. Email: gburgos@pitt.edu (G.G.-B.), lewisda@upmc.edu (D.A.L.)

Development of inhibition onto pyramidal cells may be crucial for the emergence of cortical network activity, including gamma oscillations. In primate dorsolateral prefrontal cortex (DLPFC), inhibitory synaptogenesis starts in utero and inhibitory synapse density reaches adult levels before birth. However, in DLPFC, the expression levels of γ-aminobutyric acid (GABA) synapse-related gene products changes markedly during development until young adult age, suggesting a highly protracted maturation of GABA synapse function. Therefore, we examined the development of GABA synapses by recording $GABA_A$R-mediated inhibitory postsynaptic currents ($GABA_A$R-IPSCs) from pyramidal cells in the DLPFC of neonatal, prepubertal, peripubertal, and adult macaque monkeys. We found that the decay of $GABA_A$R-IPSCs, possibly including those from parvalbumin-positive GABA neurons, shortened by prepubertal age, while their amplitude increased until the peripubertal period. Interestingly, both $GABA_A$R-mediated quantal response size, estimated by miniature $GABA_A$R-IPSCs, and the density of $GABA_A$R synaptic appositions, measured with immunofluorescence microscopy, were stable with age. Simulations in a computational model network with constant GABA synapse density showed that the developmental changes in $GABA_A$R-IPSC properties had a significant impact on oscillatory activity and predicted that, whereas DLPFC circuits can generate gamma frequency oscillations by prepubertal age, mature levels of gamma band power are attained at late stages of development.

Keywords: cognitive function, dorsolateral prefrontal cortex, GABA, gamma oscillations, inhibition, inhibitory postsynaptic current, nonhuman primate

Introduction

The development of γ-aminobutyric acid (GABA)-mediated inhibition may significantly shape the maturation of cortical network activity, including gamma band oscillations (Buzsaki and Wang 2012). In rodent neocortex, inhibitory synaptogenesis is mainly postnatal, rapidly achieving adult-like levels of inhibitory synapse density before adolescence begins (Micheva and Beaulieu 1996; De Felipe et al. 1997). Moreover, the time course of functional maturation of GABA synapses in rodents is very similar to that of inhibitory synaptogenesis, since inhibitory postsynaptic current (IPSC) frequency becomes significant only after birth, and IPSCs attain mature properties well before the onset of adolescence (Le Magueresse and Monyer 2013).

In contrast to rodents, inhibitory synaptogenesis in primate neocortex begins in utero, and adult levels of inhibitory synapse density are reached before birth, remaining stable thereafter (Bourgeois and Rakic 1993; Bourgeois et al. 1994). These observations are consistent with other findings showing that in primates many fundamental neurodevelopmental events are completed in utero (Workman et al. 2013). Thus, if the developmental trajectories of inhibitory synaptogenesis and maturation of GABA synapse function in primate neocortex were parallel, as in rodents (Le Magueresse and Monyer 2013), then in primates GABA synapses would be predicted to reach adult-like functional state before birth, when GABA synapse density reaches adult-like levels. Thus, by analogy with rodents, the functional properties of GABA synapses in primate neocortex would be expected to not change substantially during postnatal development.

The dorsolateral prefrontal cortex (DLPFC) is a region of the human and monkey neocortex among the last to achieve a fully mature state (Gogtay et al. 2004), and that lacks a clear analog or homolog in rodents (Preuss 1995). Interestingly, in the DLPFC the expression of GABA synapse-related gene products that may regulate IPSC properties continues to change during adolescence and into young adulthood (Hoftman and Lewis 2011; Catts et al. 2013; Datta et al. 2015). These data suggest that in primate DLPFC the functional maturation of GABA synapses follows a protracted postnatal trajectory, even though inhibitory synaptogenesis is complete before birth.

Since compared with mature cortex, immature inhibitory cortical circuits display higher plasticity (Maffei et al. 2010), a protracted maturation of synaptic inhibition would imply a prolonged time window during which environmental and genetic factors can shape cortical circuit development. A protracted sensitive window to the effects of such factors would suggest significant differences with rodents, in which sensitive periods typically close prior to the onset of adolescence (Hensch 2005). Therefore, a protracted primate-unique postnatal trajectory is highly significant for developmental models of schizophrenia which suggest that abnormal cortical circuit maturation contributes to cognitive dysfunction in the disease (Hoftman and Lewis 2011; Catts et al. 2013).

The IPSC peak amplitude and duration are important determinants of the power and frequency of inhibition-based oscillations, by controlling the probability of inhibiting postsynaptic neuron firing and the timing of synchronous postsynaptic firing once inhibition decays (Whittington et al. 2011). In rodents, IPSC amplitude and duration change significantly during development before adolescence (Le Magueresse and Monyer 2013) and gamma oscillations also develop rapidly

(Khazipov et al. 2013). In human cortex, gamma oscillations emerge in childhood and continue to mature until early adulthood (Uhlhaas et al. 2010). However, neither the maturation of oscillatory activity nor the functional development of GABA synapses have been examined in the human or monkey DLPFC. Thus, currently it is not known if in primate DLPFC GABA synapse function and inhibition-based rhythms mature prenatally, as would be predicted from rodent studies, or following a protracted postnatal trajectory, as predicted by the developmental changes in GABA-related gene products in humans and monkeys (Hoftman and Lewis 2011; Catts et al. 2013; Datta et al. 2015).

Here, we mapped the developmental trajectory of IPSC properties in Layer 3 pyramidal cells (PCs) of monkey DLPFC, to test if, consistent with previous molecular findings, synaptic inhibition changes substantially between the early postnatal period and young adulthood. Moreover, the impact of the developmental changes in IPSC properties on oscillatory network activity was evaluated in a computational network model, to generate predictions that can be tested in future experimental studies.

Materials and Methods

Brain Slice Preparation

Electrophysiology experiments were carried out with tissue obtained from 10 female rhesus monkeys (*Macaca mulatta*), experimentally naïve until entry into this study. Five animals were bred at the University of Pittsburgh Primate Research Center, and the others were acquired from vendors. Animals were housed with their mothers until 6 months of age when they were placed by groups in the same social setting. Older animals were housed either in pairs or in single cages in the same setting. Animals were divided into 4 age groups (Plant 1988): Neonatal (1.2, 1.3, and 1.5 months); 2) Prepubertal (9.5 and 12.5 months); 3) Peripubertal (32.7, 34.2, and 34.8 months), and 4) Adult (59.5 and 64.1 months). All housing and experimental procedures were conducted in accordance with US Department of Agriculture and National Institutes of Health guidelines as approved by the University of Pittsburgh Institutional Animal Care and Use Committee.

Tissue blocks containing DLPFC areas 9 and 46 were obtained from one or both cerebral hemispheres of each animal. The neonatal animals and the 32.7 month-old animal were deeply anesthetized and perfused transcardially with ice-cold sucrose-modified artificial cerebro-spinal fluid (sucrose-ACSF, in mM): sucrose 210, NaCl 10, KCl 1.9, Na_2HPO_4 1.2, $NaHCO_3$ 33, $MgCl_2$ 6, $CaCl_2$ 1, glucose 10 and kynurenic acid 2; pH 7.3–7.4 when bubbled with 95% O_2–5% CO_2. The brain was rapidly removed and bilateral DLPFC blocks were prepared. For all other animals, an initial DLPFC tissue block was removed from one hemisphere as described (Gonzalez-Burgos et al. 2008) and a second contralateral tissue block was removed 1–2 weeks later, using the transcardial cold sucrose-ACSF perfusion procedure described above. When 2 tissue blocks were removed per animal in separate procedures, the locations of the blocks were off-set in the rostral-caudal axis to study nonhomotopic portions of the DLPFC from each hemisphere. We previously showed that the first procedure does not alter the physiological or anatomical properties of neurons in the tissue obtained in the second hemisphere (Henze et al. 2000). Coronal DLPFC slices (300 µm thick) were cut using a vibrating microtome (VT1000S, Leica Microsystems) in ice-cold sucrose-ACSF. Immediately after cutting, slices were transferred to an incubation chamber at room temperature filled with the following ACSF (mM): NaCl 126, KCl 2, Na_2HPO_4 1.2, glucose 10, $NaHCO_3$ 25, $MgCl_2$ 6 and $CaCl_2$ 1, pH 7.3–7.4 when bubbled with 95% O_2–5% CO_2.

Electrophysiological Recordings

Slices were placed in a recording chamber superfused at 2–3 mL/min with the following ACSF (mM): NaCl 126; KCl 2.5; Na_2HPO_4 1.2; $NaHCO_3$ 25; glucose 10; $CaCl_2$ 2; $MgCl_2$ 1; CNQX 0.01, bubbled with 95% O_2/5% CO_2 at 30–32 °C. Whole-cell recordings were obtained from Layer 3 PCs visually identified using infrared differential interference contrast video microscopy in either medial or lateral banks of the principal sulcus in Area 46. Recording pipettes had 3–5 MΩ resistance when filled with the following solution (mM): CsCl 120; NaCl 10; ethyleneglycol-bis(2-aminoethylether)-*N*,*N*,*N*′,*N*′-tetra acetic acid (EGTA) 0.2; 4-(2-hydroxyethyl)-1-piperazineethanesulfonic acid (HEPES) 10; MgATP 4; NaGTP 0.3, NaPhosphocreatine 14, biocytin 0.5%, pH 7.2–7.3. Voltage clamp recordings were performed using Multiclamp 700 amplifiers (Axon Instruments). The series resistance (≤18 MΩ) was not compensated but was continuously monitored using a small voltage step (20 ms, 5 mV) and recordings were excluded from the data analysis if the series resistance changed >15%. IPSCs were recorded at a holding potential of −80 mV in the presence of 10 µM CNQX. For miniature IPSC (mIPSC) recordings, 1 µM tetrodotoxin was added and its effects monitored via blockade of the action currents (i.e., the currents associated with action potentials triggered via voltage escape during large depolarizing voltage commands). Signals were low-pass filtered at 4 kHz, digitized at 10 or 20 kHz, and stored on disk using Signal 5 software (Cambridge Electronic Design). Current clamp recordings and data analysis were done as described previously (Henze et al. 2000; Gonzalez-Burgos et al. 2004; Zaitsev et al. 2012), with Multiclamp 700 amplifiers operating in bridge mode with pipette capacitance compensation, using the following pipette solution (mM): KGluconate 120.0; NaCl 10.0; EGTA 0.2; HEPES 10.0; MgATP 4.0; NaGTP 0.3, NaPhosphocreatine 14, pH 7.2–7.3. Current clamp recordings were included in data analysis only if the resting membrane potential was ≤−60 mV. To study the cells' membrane properties and firing pattern, current steps (500 ms, −80 to 600 pA) were delivered through the recording electrode. All reagents were from Sigma-Aldrich, except agatoxin IVA (Bachem). Analysis of data from current clamp recordings is described in Supplementary Methods.

Spontaneous IPSC (sIPSC) and mIPSC data analysis. sIPSCs and mIPSCs were analyzed starting 2–5 min from the beginning of whole-cell recording. Events (sIPSCs or mIPSCs) were detected with MiniAnalysis software (Synaptosoft) using both amplitude and area thresholds. To obtain an average sIPSC or mIPSC for each recorded neuron, we used validation by 2 steps of visual inspection of the detected events. First, events were inspected in 1-s-long time windows to find consecutive events with overlap of decay and rising phases. Second, the rising phase of the events was inspected at an expanded time window (10 ms-long, starting at a baseline time point 5 ms prior to event onset) to detect inflections in the rising phase. Whereas all detected events were used to compute IPSC frequency, overlapping events and events with inflections in the rising phase were eliminated from the average. The sIPSC and mIPSC database typically contained 50–200 events per PC. To obtain an average sIPSC or mIPSC, events were aligned from the baseline current via their rising phase and onset (see Fig. 1*C*). The rise time, amplitude and decay time constant of the average IPSC were estimated using MiniAnalysis or Signal software scripts. The IPSC decay time was fitted with either a single exponential decay or with the sum of 2 exponential functions, in which case a weighted decay time constant was computed as $\tau w = (Af \times \tau f + As \times \tau s)/(Af + As)$, where Af and τf are the amplitude and time constant of the fast decay component and As and τs are the respective values of slow decay. Whereas a double exponential decay in some cases improved the fit compared with a single exponential, the weighted decay time constants did not differ significantly from the single exponential decay time constants and the significance of the effect of age on IPSC decay was unaltered by the exponential decay model function used to fit the IPSC decay.

IPSCs evoked with extracellular stimulation. Previous studies have suggested that perisomatic extracellular stimulation elicits IPSCs originating predominantly, although not exclusively, from interneurons furnishing perisomatic GABA synapses (Kruglikov and Rudy 2008; Gonzalez-Burgos et al. 2009). Importantly, most of the synaptic contacts originating from perisomatic-targeting interneurons target proximal basal and apical dendrites rather than the pyramidal cell soma (Somogyi et al. 1998). Bipolar perisomatic extracellular stimulation was delivered

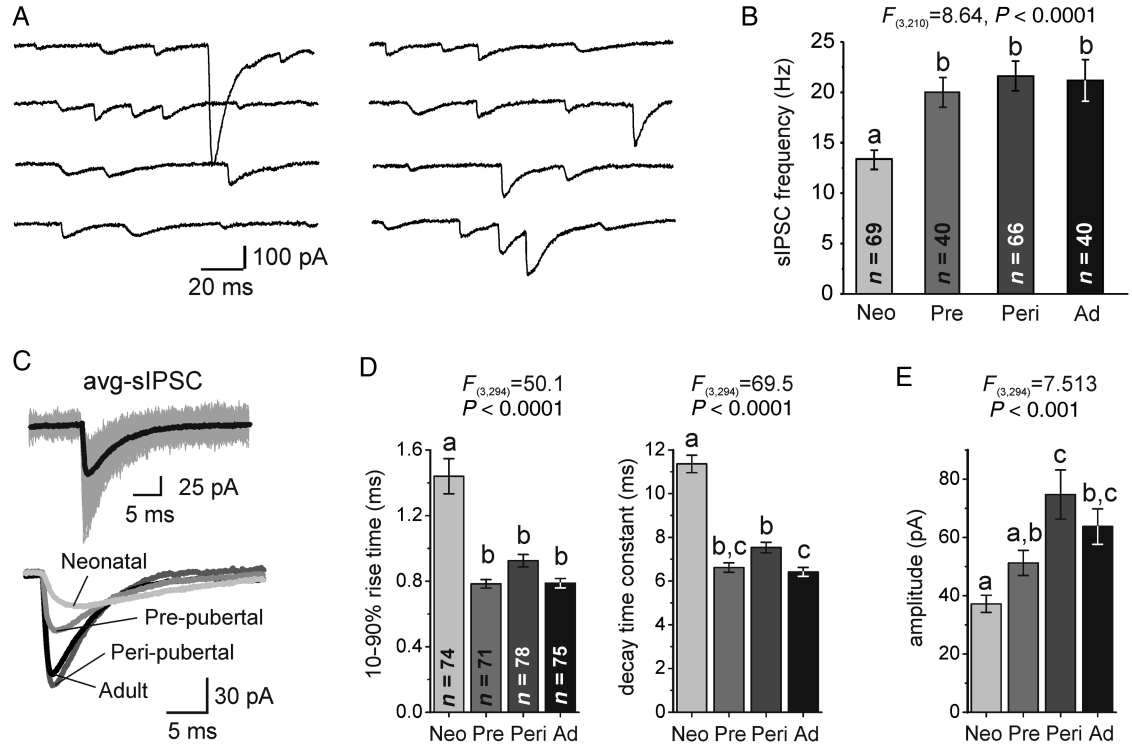

Figure 1. Spontaneous $GABA_AR$-mediated IPSCs (sIPSCs) in Layer 3 PCs. (*A*) Representative recordings of sIPSCs from a neonatal PC. sIPSCs were blocked after adding the $GABA_AR$ antagonist gabazine (Supplementary Fig. 1). (*B*) Quantification of sIPSC frequency in all age groups. Here and in all other figures, bars not sharing the same letter are significantly different at $P < 0.05$, Bonferroni post hoc comparison tests. Age groups are abbreviated as: neonatal, Neo; prepubertal, Pre; peripubertal, Peri; adult, Ad. (*C*) Top: Representative average sIPSCs (avg-sIPSC, black) together with multiple individual sIPSCs superimposed (gray). Bottom: representative avg-sIPSCs from PCs of the different age groups. (*D*) Quantification of sIPSC 10–90% rise time and sIPSC exponential decay time constant. (*E*) Quantification of avg-sIPSC amplitude.

with theta-glass pipettes (open tip diameter 2–3 μm) filled with oxygenated ACSF, connected via silver wires to a stimulus isolator (World Precision Instruments) and placed near the soma (~20–50 μm) of the recorded PC. The amplitude of the stimulus pulses (100 μs duration), was adjusted (30–150 μA) to elicit perisomatic IPSCs (pIPSCs) of the smallest possible amplitude without failures, at a baseline stimulus frequency of 0.2 Hz. After recording pIPSCs for 10 min, 250 nM ω-agatoxinIVA was applied and the recording continued until a stable effect of agatoxin was observed. To obtain the agatoxin-resistant pIPSC waveform (agaR-pIPSC), 10–20 consecutive agaR-pIPSCs were averaged. The agatoxin-sensitive pIPSC (agaS-pIPSC) was obtained averaging 10–20 pIPSCs recorded just before agatoxin application and subtracting from this waveform the agaR-pIPSC (Fig. 6*A*).

Computational Network Model and Simulations

The model consists of a network of 50 excitatory cells (E) and 20 inhibitory (I) spiking neurons. Each E and I cell is connected to every other E and I cell with a random strength drawn from a uniform distribution and divided by the number of inputs. Each neuron obeys the following dynamics (Izhikevich 2004):

$$C\frac{dV}{dt} = I_{appl} + g_l\frac{(V-V_l)(V-V_T)}{V_T-V_l} - z\,(V-V_K) - I_{syn} + \sigma N$$

$$\frac{dz}{dt} = -az$$

Where z represents adaptation $a = 1(/80$ ms), and N is a small amount of white noise ($\sigma = 0.05$) added to E and I cells. A random tonic drive (I_{appl}, 3–5 μA/cm^2) drives the E cells only, thus I cells only fire if E cells fire. Each time $V(t)$ hits V_{spike}, z is incremented by d and V is reset to V_r. For E cells, $g_l = 0.1$, $V_l = -65$, $V_T = -50$, $V_r = -70$, $d = 0.05$, $V_{spike} = 20$, $V_K = -85$. I cells are the same, but $V_r = -60$ and $d = 0$ (no spike frequency adaptation). $C = 1$ μF/cm^2, all conductances are in mS/cm^2, voltages are in mV.

Parameters are chosen so that at rest E cells have a membrane time constant of 20 ms and I cells 10 ms. Synaptic currents have the form:

$$I_{syn} = (g_e s_e + g_n s_n)(V - V_{ex}) + g_i s_i\,(V - V_{in})$$

Where $V_{in} = -70$, $V_{ex} = 0$. Every neuron to which a given cell is connected to, contributes its own synaptic current. The synaptic gating variables satisfy:

$$\frac{ds_e}{dt} = -s_e/\tau_e$$

$$\frac{ds_n}{dt} = a_n\,s_e\,(1-s_n) - s_n/\tau_n$$

$$\frac{ds_i}{dt} = -s_i/\tau_i$$

Here s_e, s_n, and s_i are alpha-amino-3-hydroxy-5-methyl-4-isoxazole propionic acid (AMPA), *N*-methyl-D-aspartate (NMDA), and GABA synapses, respectively. The model for NMDA does not include Mg^{2+} block (Rotaru et al. 2011). Each time an E cell fires, s_e is incremented by 1; each time an I cell fires, its corresponding s_i is incremented by 1. For E–E and E–I connections, $g_{ee} = g_{ei} = 1$, $g_{ne} = 0.25$, $g_{ni} = 0.1$, $\tau_{ee} = \tau_{ei} = 2$ ms, $\tau_{ne} = \tau_{ni} = 80$ ms. For I–E and I–I connections, g_{ie} varied from 0.2 to 2.2, $g_{ii} = 1$, τ_{ie} varied from 20 to 1 ms and $\tau_{ii} = 7$ ms. All simulations were performed using XPPAUT; the code is available from the authors. Euler's method was used with a step size of 0.05 ms. Power spectra were taken on the s_e, the E–E synaptic gating variable, which is the sum of all the excitatory currents into the excitatory cells. Rasters are plots of s_e.

Statistical Analysis

Data are presented as mean ± SE. Differences between group means were tested, except when otherwise mentioned, using Student's *t*-test or ANOVA followed by Bonferroni post hoc tests. For ratios or

percentages, which do not follow a normal distribution, logarithmic transformations were performed before the statistical tests. The analysis of sIPSC rise time and amplitude used mixed models where log (rise time) and log(amplitude) were modeled with age group as a fixed effect and neuron as a random effect, to account for repeated measurements made on the same neuron (dependence among neurons from the same monkey was highly insignificant). To determine possible differences between age groups simultaneously in sIPSC rise time and amplitude, the null hypothesis that sIPSC rise time and amplitude are the same for 2 successive age groups was rejected at 0.05/3 level if either log(rise time) and log(amplitude) differed at 0.025/3 level between the 2 successive ages, thus protecting the multiple tests' Type 1 error rate. An additional supportive analysis of sIPSCs was done defining a 97.5% probability contour for the distribution of sIPSC rise time and amplitude in the neonatal group, where this contour is based on a bivariate normal distribution with a suitably estimated mean and covariance matrix. To better understand the differences in the joint distribution of rise time and amplitude over the age groups, the probability of an sIPSC being within the neonatal contour was compared between the other age groups and the neonatal group at nominal 0.05 levels using a logistic mixed model with age group as a fixed effect and neuron as a random effect. Further details about the methodology are described in Supplementary Methods.

Reconstruction of Biocytin-Filled Neurons

Layer 3 pyramidal neurons were filled with 0.5% biocytin during recording, after which the slices were immersed in 4% *p*-formaldehyde in 0.1 M phosphate-buffered saline (PBS) for 24–72 h at 4°C, then cryoprotected (33% glycerol, 33% ethylene glycol, in 0.1 M PBS) and stored at −80°C until processed for visualization of the biocytin label. Slices were resectioned at 60 µm, incubated with 1% H_2O_2, immersed in blocking serum containing 0.5% Triton X-100 for 2–3 h at room temperature, rinsed, and incubated with the avidin–biotin–peroxidase complex (1:100; Vector Laboratories) in PBS for 4 h at room temperature. Sections were rinsed, stained with the Nickel-enhanced 3,3′-diaminobenzidine chromogen, mounted on gelatin-coated glass slides, dehydrated, and coverslipped. Three-dimensional reconstructions and quantitative morphometry of the dendritic tree of layer 3 pyramidal cells, were performed using the Neurolucida neuron tracing system and NeuroExplorer software (MBF Bioscience).

Immunohistochemistry and Confocal Microscopy

Immunohistochemistry and confocal microscopy were done in tissue obtained from 3 neonatal monkeys (1.3 month-old female; 0.6 and 0.7 month-old males) bred at the University of Pittsburgh Primate Research Center and 3 peripubertal monkeys (39, 42, and 46 month-old males) obtained from other sources.

Antibodies and immunocytochemistry. Two sections per monkey, localized 1 mm apart in the middle third of the principal sulcus in area 46, were multi-labeled for 1) PV (sheep, R&D Systems; 1:100) (Kagi et al. 1987) and the vesicular GABA transporter (vGAT; guinea pig, Synaptic Systems; 1:500) (Guo et al. 2009) to identify presynaptic terminals; 2) the $GABA_A$ receptor subunit gamma 2 (γ2; rabbit, Synaptic Systems; 1:400) (Fritschy and Mohler 1995) to identify postsynaptic sites; and 3) neuronal nuclei (NeuN; mouse, Millipore; 1:500) (Mullen et al. 1992) to identify PC soma. The specificity of each primary antibody was verified as described previously (Fish et al. 2013). Secondary antibodies (Donkey) were conjugated to Alexa 405, 488, 568, 647 (Invitrogen), or biotin (Fitzgerald). A tertiary incubation with streptavidin 405 was performed to label the biotinylated secondary antibody. The final fluorescence detection channel assignment (excitation) was: vGAT (405 nm), NeuN (488 nm), PV (568 nm), and GABAA γ2 (647 nm).

Acquisition of images. Image stacks (512 × 512 pixels; 0.25 µm *z*-step) were collected using a ×60 1.42 NA objective on an Olympus IX71 microscope controlled by SlideBook 5.0 (3I) and equipped with an Olympus DSU spinning disk and a ×60 SC 1.42 NA objective. The microscope was equipped with a Hamamatsu C9100 EM-CCD camera, and a LEP BioPrecision2 *XYZ* motorized stage. Sampling was confined to deep Layer 3, defined as 35–50% of the distance from pial surface to white matter. Sites were systematically sampled using a grid of 190 × 190 µm with stacks collected from 20 randomly selected sites per section. The virtual sampling box started and ended one *z*-plane from the top and bottom of the image stack, respectively, and had *x*–*y* start/end coordinates that were located 20 pixels from any edge.

Image Processing

Image stacks were taken using optimal exposures (greatest dynamic range/no saturated pixels), exposure corrected, deconvolved using the AutoQuant adaptive blind deconvolution algorithm, and segmented. A custom threshold/morphological segmentation algorithm was used to create object masks of the immunoreactive (IR) puncta. This segmentation algorithm used the Ridler–Calvard iterative thresholding method (Ridler and Calvard 1978) to obtain an initial value for iterative segmentation. The Ridler–Calvard method chooses an initial threshold based on the assumption that the histogram for each channel is the sum of the distributions for both signal and background pixels, and then iteratively calculates a new threshold by taking the mean of the average intensities of the signal and background pixels determined by the initial threshold. This process is repeated until the threshold converges. For optimal masking of pre- and postsynaptic structures, 100 iterations with subsequent threshold settings increasing by 50 gray levels were performed.

Definitions of Synaptic Structures

Intensity/morphological segmentation was used to make masks for each IR puncta, identified as small (0.03–1 μm^3), distinct fluorescing objects (Fish et al. 2013). Labeling for vGAT, which concentrates in GABAergic terminals (Chaudhry et al. 1998), was used to classify IR puncta as GABAergic terminals (vGAT-IR). Mask operations in SlideBook were then used to classify the different terminal populations. For example, a PV object mask that contained the center of a vGAT object mask was defined as a PV terminal (PV/vGAT-IR). Appositions between putative pre- and postsynaptic structures were identified where the fluorescent signal mask from labeled terminals (vGAT-IR or PV/vGAT-IR) overlapped with that from $GABA_A$ receptor γ2-IR puncta (vGAT/ γ2 apposition or vGAT/PV/ γ2 apposition, respectively). All vGAT-IR puncta that overlapped with γ2-IR puncta were classified as being either a vGAT/γ2 apposition or vGAT/PV/γ2 apposition. Threshold segmentation of the NeuN signal was used to create a mask object for the PC soma.

Statistical Analysis of Synaptic Apposition data

Diagnostic statistics were used to confirm that the data were normally distributed. Independent *t*-tests were used to compare apposition densities, numbers of vGAT/γ2 apposition and vGAT/PV/γ2 appositions, and fluorescence intensity data between age groups. In all analyses, the statistics were performed on the mean values for individual monkeys ($n = 3$ per age group) determined by first averaging data within stack, then averaging stack means within section, and finally averaging means across sections.

Results

Spontaneous and Miniature IPSC Properties Change Significantly During Postnatal Development

In monkey DLPFC, inhibitory synaptogenesis begins in utero, and the mean inhibitory synapse density displays adult levels before birth (Bourgeois et al. 1994). Here we found that Layer 3 DLPFC PCs from neonatal (~1 month-old) monkeys displayed frequent $GABA_AR$-mediated spontaneous IPSCs (sIPSCs, Fig. 1*A* and Supplementary Fig. 1A), suggesting that a significant fraction of neonatal GABA synapses are functional. The sIPSC frequency increased between neonatal and prepubertal age (9–12 months old) and remained higher in

peripubertal (~34 month-old) and adult (~64 month-old) neurons (Fig. 1*B*). The 10–90% rise time and the decay time constant of average sIPSCs (avg-sIPSCs, Fig. 1*C*) decreased between neonatal and prepubertal ages, and remained shorter thereafter (Fig. 1*D*). Moreover, the avg-sIPSC amplitude increased in PCs from peripubertal animals and remained larger in adult animals (Fig. 1*E*). These findings indicate that $GABA_A$-R-mediated IPSCs in layer 3 PCs of DLPFC change substantially during postnatal development.

In PCs from all age groups, sIPSCs had heterogeneous rising slopes and amplitudes (Fig. 1*A*). Individual IPSCs with both shorter rise time and larger amplitude likely originate from synapses at or near the soma (Xiang et al. 2002; Lazarus and Huang 2011; Goswami et al. 2012), where the membrane potential is better controlled by the somatic voltage-clamp and dendritic filtering is less significant (Williams and Mitchell 2008). The age-related changes in avg-sIPSCs may thus reflect, among other possibilities, a greater proportion of sIPSCs from perisomatic GABA synapses. We therefore compared the joint distributions of sIPSC amplitude and 10–90% rise time measured in individual synaptic responses. The sIPSC distributions for the PC population in each age group showed an increase with age in the proportion of sIPSCs with larger amplitude and shorter rise time (Fig. 2*A*). The age-related changes in sIPSC distributions were similarly observed in single neurons, since individual PCs from adult monkeys consistently displayed

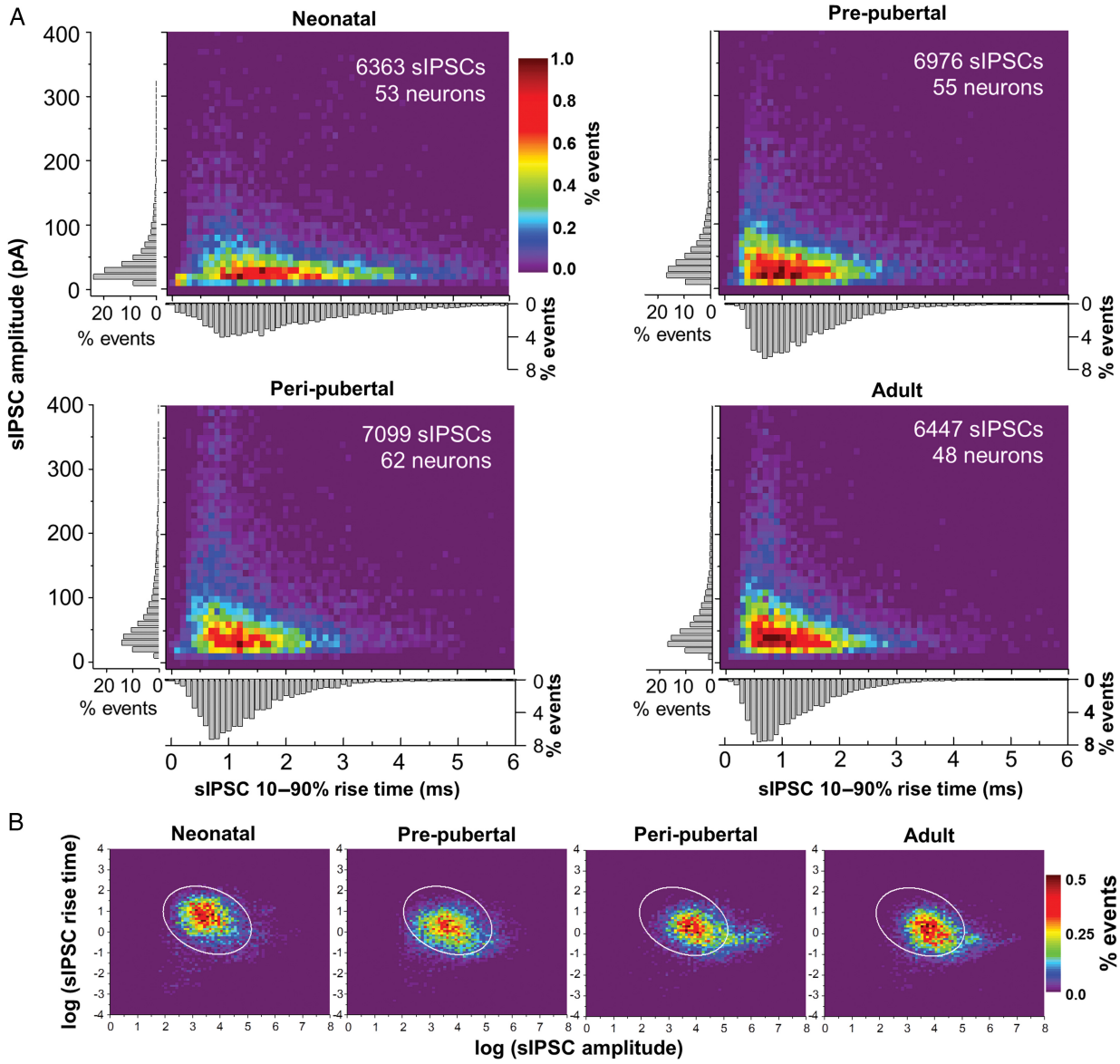

Figure 2. Analysis of sIPSC rise time and amplitude distribution. (*A*) Distribution histograms for sIPSCs across age groups. The color-coded scale of relative frequency (percentage of events) applies to all age groups. A bivariate mixed model revealed significant differences in distribution between neonatal versus prepubertal ($P < 0.0001$), prepubertal versus peripubertal ($P < 0.0001$) but not peripubertal versus adult ($P = 0.1143$). The gray bar graphs next to the axes in each heatmap show the distributions of relative frequency (percentage of events) of rise time and amplitude separately. (*B*) sIPSC rise time and amplitude distribution after logarithmic transformation of the data. The color scale of percentage of events applies to all plots. The ellipse superimposed on the distribution plots is an elliptical contour that contains 97.5% of the data points in the neonatal distribution. The percentages of sIPSCs within the ellipse for an age group were compared with each other using a generalized linear model, revealing significant shifts between the neonatal group and the other 3 age groups (see Materials and methods and Supplementary Data for details on statistical analysis).

greater proportion of sIPSCs with both larger amplitude and shorter rise time (Supplementary Fig. 1*B*). Linear mixed model analysis of the data in Figure 2*A*, after a logarithmic transformation (see also Fig. 2*B*), revealed significant differences in the rise time and amplitude distribution between adjacent age groups, except for peripubertal versus adult (neonatal vs. prepubertal $P < 0.0006$; prepubertal vs. peripubertal $P < 0.0006$, peripubertal vs. adult $P = 0.330$). Our data thus show that in Layer 3 PCs the proportion of sIPSCs with both larger amplitude and shorter rise time at the soma increases with age.

Graphical approaches were also used to better understand the nature of the changes in rise time and amplitude distributions over the age groups. Subtraction of other age groups from the neonatal distribution to reveal the regions of greatest difference, confirmed the age-related shift in the sIPSC distribution towards a region with larger amplitude and shorter rise time (Supplementary Fig. 1*C*). The bivariate distributions were also compared between the neonatal and other age groups by superimposing a 97.5 probability elliptical contour based on the neonatal distribution (i.e., an ellipse containing 97.5% of the neonatal data points) on the distributions of log-transformed data for each age group (Fig. 2*B*). The percentages of sIPSCs within the ellipse were compared using a generalized linear model, which showed significant shifts between the neonatal and the other 3 age groups (neonatal vs. prepubertal, $t = -2.45$, df = 199.4, $P = 0.02$; neonatal vs. peripubertal, $t = -3.68$, df = 201.9, $P < 0.0005$; neonatal vs. adult, $t = -1.99$, df = 199.1, $P < 0.05$).

In both monkey and rat prefrontal cortex slices, some sIPSCs are produced via spontaneous action potential (AP) firing (Kroner et al. 2007; Bories et al. 2013). Because single GABAergic axons typically form multiple synaptic contacts with each target neuron (Somogyi et al. 1998), AP-evoked sIPSCs may involve synchronous GABA release from multiple contacts. Therefore, the increase in sIPSC amplitude with age could reflect a larger number of sites releasing GABA per AP, instead of a larger synaptic response to GABA. Consistent with the idea that sIPSCs involve spontaneous AP firing, miniature IPSCs (mIPSCs, Fig. 3*A,B*) recorded in the presence of 1 µM tetrodotoxin had significantly lower frequency ($F_{1,184} = 13.136$, $P < 0.0005$) than sIPSCs in the same age groups (Fig. 1*B*). The sIPSC frequency was 47% higher in peripubertal PCs (sIPSCs: 21.6 ± 1.4 Hz, $n = 66$, mIPSCs: 14.6 ± 1.2 Hz, $n = 24$, $P < 0.002$), and 35% greater, although nonsignificantly, in neonatal PCs (sIPSCs: 13.4 ± 0.9 Hz, $n = 69$, mIPSCs: 9.9 ± 0.9 Hz, $n = 29$, $P = 0.081$). These data show that a significant fraction of sIPSCs is produced via AP-evoked release.

We next studied the properties of mIPSCs, thought to reflect the GABA response at single synaptic contacts or release sites (Auger and Marty 2000), to test whether the age-related changes in sIPSCs reflect changes in the quantal synaptic response to GABA. Similar to the sIPSCs (Fig. 1), average mIPSCs (avg-mIPSCs, Fig. 3*C*) had significantly shorter rise time and decay time constant in peripubertal neurons (Fig. 3*D*). However, the avg-mIPSC amplitude did not differ ($P = 0.664$) between neonatal and peripubertal age groups (Fig. 3*E*), even though these groups had the largest difference in sIPSC amplitude (Fig. 1*E*). Moreover, the distribution of mIPSC rise time showed a significant age-related shift to shorter values, however, the distribution of mIPSC amplitude did not change with age (Fig. 3*F,G*). Interestingly, whereas the avg-sIPSC and avg-mIPSC amplitudes did not differ in neonatal PCs ($P = 0.465$), in peripubertal PCs avg-sIPSCs had ~3 times larger amplitude than avg-mIPSCs ($P < 0.0001$). Assuming that mIPSCs and sIPSCs originate from the same pool of synaptic vesicles (Hua et al. 2010), these data suggest that the increase in sIPSC amplitude is the consequence of an age-related increase in the number of synaptic contacts or release sites synchronously releasing GABA in an AP-dependent manner.

Absence of Change in Intrinsic Pyramidal Cell Properties During Postnatal Development

In rodent neocortex, both the size and complexity of pyramidal cell dendrites increase markedly during postnatal development, the total dendritic length and membrane area increasing by ~5-fold in the first 3 postnatal weeks (Zhu 2000; Zhang 2004; Etherington and Williams 2011). Dendritic tree size is a major determinant of electrical coupling between dendrites and soma (Zhu 2000), including in Layer 3 PCs of monkey DLPFC (Amatrudo et al. 2012). Thus, age-related changes in dendritic morphology could produce different space-clamp errors and dendritic filtering, generating differences in IPSC properties independent of actual synapse properties (Williams and Mitchell 2008). Importantly, in striking contrast to the rodent cortex, a previous Golgi impregnation study showed that in Layer 3 PCs of monkey DLPFC dendritic tree size and complexity are stable between 1 week postnatal and adulthood (Anderson et al. 1995). Consistent with these previous data, in reconstructions of Layer 3 PCs filled with biocytin during recording (Fig. 4*A*), we found that neither the apical or basal dendritic tree length (Fig. 4*B*) nor the number of primary basal dendrites changed with age (basal dendrites per PC, neonatal: 6.4 ± 0.7; prepubertal: 7.8 ± 0.9; peripubertal: 7.7 ± 0.8; adult: 6.7 ± 0.5; $F_{3,18} = 0.903$, $P = 0.459$). Moreover, dendritic tree complexity assessed by Sholl analysis did not differ between age groups (Fig. 4*C*).

Besides dendritic tree morphology, developmental changes in passive membrane properties may affect the electrical coupling between dendrites and soma. However, large changes in the specific membrane resistance, specific membrane capacitance, or intracellular resistivity are necessary to modify dendrite–soma coupling when dendrite morphology is constant (Stuart and Spruston 1998). Dendrite–soma coupling is also dependent on the active properties of the PC membrane, which in rodent cortex change significantly during early postnatal development, in parallel to the rapid maturation of PC morphology (Zhu 2000; Zhang 2004; Etherington and Williams 2011). We thus examined the intrinsic electrophysiological properties of neonatal and peripubertal Layer 3 PCs using somatic current clamp recordings (Fig. 4*D,E*). Interestingly, neither input resistance, membrane time constant, single AP properties or firing pattern differed between Layer 3 PCs from neonatal and peripubertal monkeys (Table 1 and Fig. 4*D,E*), and were very similar to those previously reported for adult monkeys (Gonzalez-Burgos et al. 2004; Amatrudo et al. 2012; Zaitsev et al. 2012). Therefore, our data suggest that layer 3 PCs have mature morphological and electrophysiological properties at neonatal age (~1 month).

GABA Synaptic Apposition Number is Stable During Postnatal Development

In rodent cortex, the number of synaptic contacts between each GABAergic axon and target cell and the number of

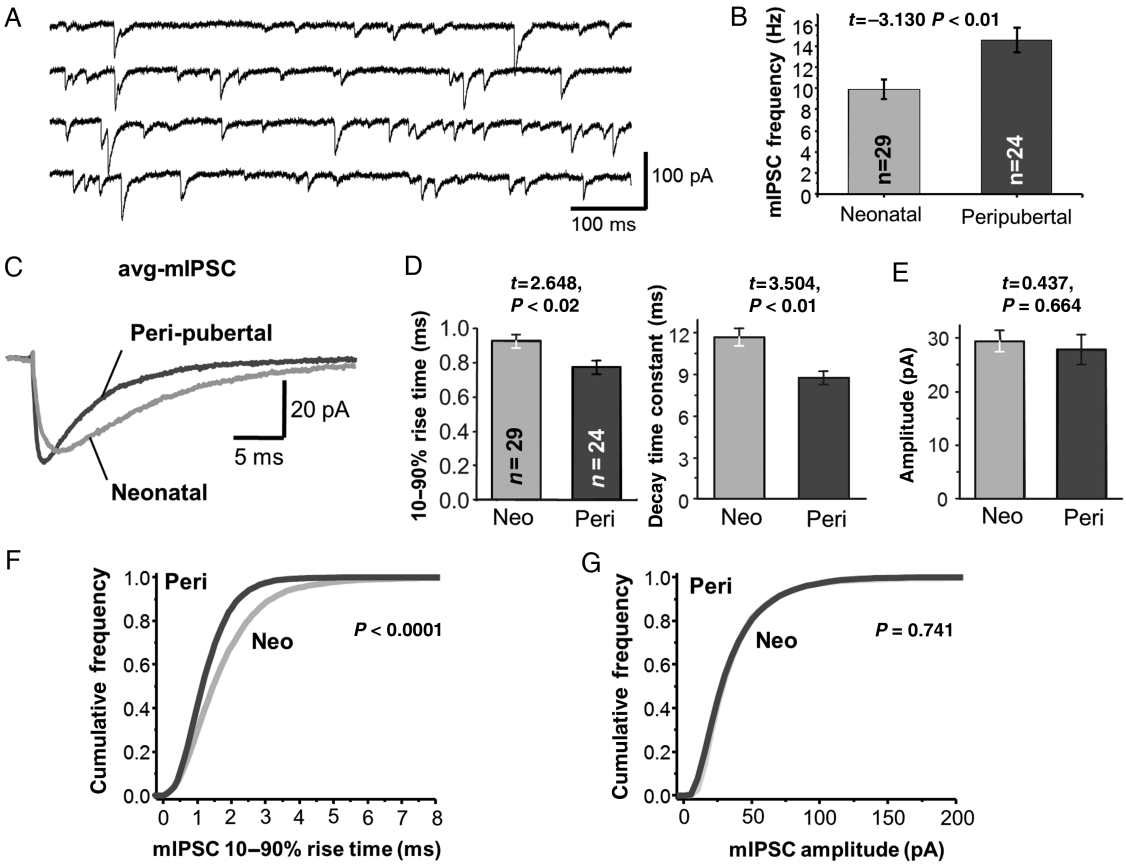

Figure 3. Analysis of miniature $GABA_AR$-mediated IPSCs (mIPSCs) in Layer 3 PCs. (*A*) Examples of mIPSC recordings from a neonatal Layer 3 PC. (*B*) Quantification of the mIPSC frequency in neonatal and peripubertal neurons. (*C*) Representative average mIPSCs (avg-mIPSCs) generated for PCs in slices from neonatal and peripubertal animals. (*D*) Quantification of the avg-mIPSC 10–90% rise time and exponential decay time constant. (*E*) Quantification of mIPSC amplitude. (*F*) Cumulative frequency distribution of mIPSC 10–90% rise time in neonatal and peripubertal neurons. Significance of differences with age was assessed via Kolmogorov–Smirnov test. (*G*) Cumulative frequency distribution of mIPSC amplitude.

neurons targeted by each axon, increase during postnatal development (Chattopadhyaya et al. 2004). A similar development of GABAergic innervation could explain the age-related increase in sIPSC amplitude we found in Layer 3 PCs, however inhibitory synapse density in monkey DLPFC is at adult levels at the time of birth and does not change postnatally (Bourgeois et al. 1994). Still, GABAergic innervation could increase in some compartments of the PC membrane and decrease elsewhere, without changing the total number of GABA synapses, as determined using electron microscopy (Bourgeois et al. 1994). Therefore, to examine if GABAergic innervation of Layer 3 PC somas changes with age, we measured the density of appositions between GABAergic boutons and somatic $GABA_AR$ clusters (Fig. 5*A*,*B*) in DLPFC tissue sections from neonatal (1 month-old) and peripubertal (42 month-old) monkeys. As described elsewhere (Fish et al. 2013), we imaged puncta immunolabeled for parvalbumin (PV, present in synapses from PV-positive neurons, Fig. 5*A*,*Ca*), the postsynaptic $GABA_AR$ gamma 2 subunit (γ2, found in most $GABA_A$-Rs, Fig. 5*A*,*Cb*) and vGAT (vesicular GABA transporter, Fig. 5*A*, *Cc*). For each puncta we created a mask object (Fig. 5*Da–c*) by processing the images with a custom segmentation algorithm. Putative synaptic appositions were identified via overlap of mask objects (Fig. 5*A*,*Cd*,*Dd*). We found that neither the density of vGAT/γ2 (PV-negative) nor vGAT/PV/γ2 (PV-positive) somatic appositions differed between neonatal (1 month-old) and peripubertal (42 month-old) animals (Fig. 5*E*,*F*). In addition, the mean fluorescence intensity for vGAT and γ2 proteins did not differ between age groups in vGAT/γ2 or vGAT/PV/γ2 somatic appositions (Table 2), suggesting that vGAT and γ2 protein levels per soma apposition do not differ with age. In contrast, the mean PV protein levels in somatic vGAT/PV/γ2 appositions were significantly higher in the peripubertal age group (Fig. 5*G*,*H*). Interestingly, when all GABA synaptic appositions (not specifically restricted to PC soma) were analyzed, neither the total number of appositions (Supplementary Table 1) nor the vGAT or γ2 mean protein levels differed between age groups, whereas PV levels increased with age (Supplementary Table 2). These data, in concert with our recent study of 3 month-old and adult monkeys (Fish et al. 2013), suggest that perisomatic GABAergic innervation of PCs reaches a mature state at an early postnatal age, as predicted by previous electron microscopy studies (Bourgeois et al. 1994).

Perisomatic IPSC Duration Shortens and Amplitude Increases During Postnatal Development

If the mean number of perisomatic GABA synapses is stable between neonatal and adult age (Fig. 5), then the increased proportion of large sIPSCs with short rise time (Fig. 2) is unlikely to be associated with an increase in perisomatic synapse number. Instead, the rise time may shorten with age in IPSCs

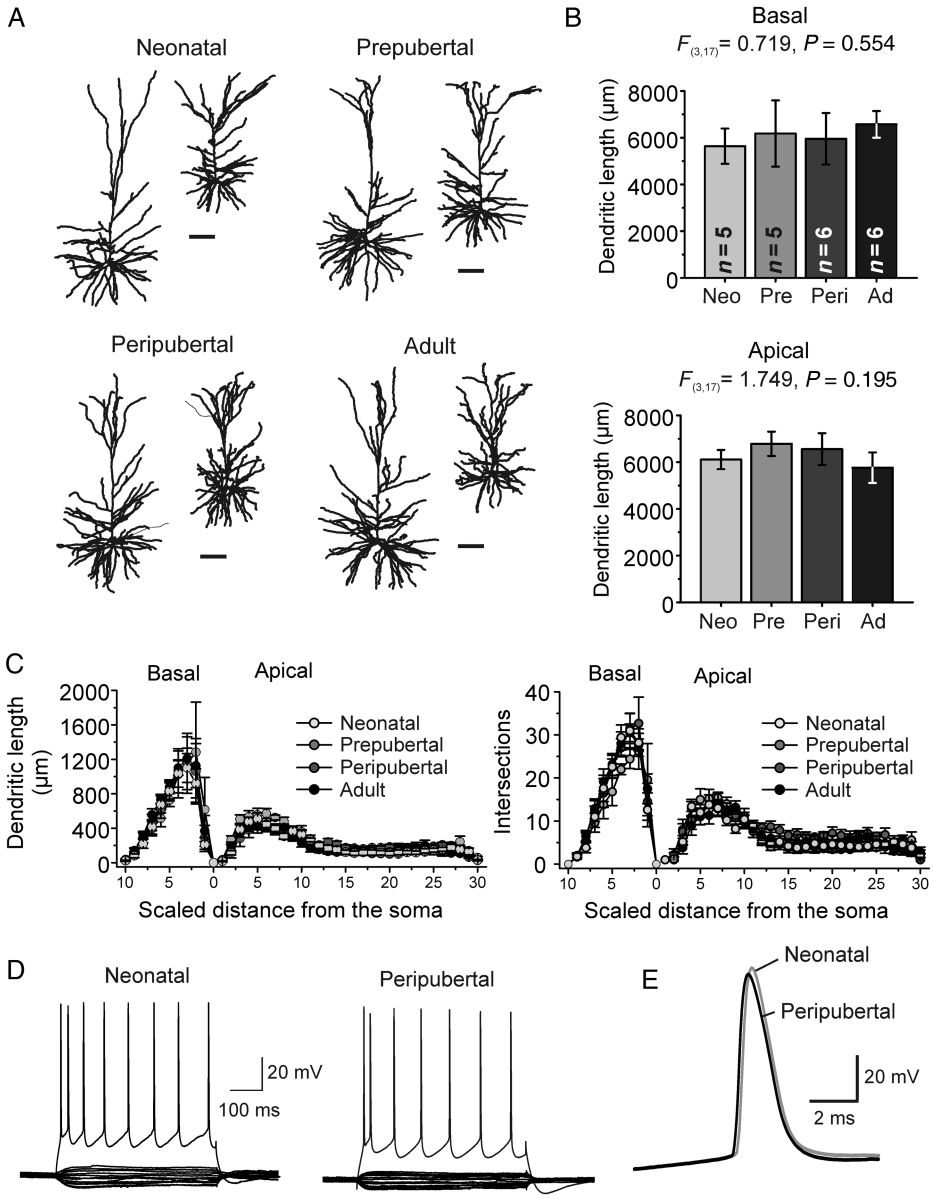

Figure 4. Dendritic morphology and membrane properties of Layer 3 PCs in monkey DLPFC. (*A*) Representative 3D Neurolucida reconstructions of the apical and basal dendrites. Scale bars: 100 µm. (*B*) Quantification of total basal and apical dendritic length. (*C*) Sholl analysis of dendritic length (left) and intersections (right) as a function of normalized distance from the soma, for basal and apical dendrites. The distance between Sholl rings was adjusted for each PC so that 10 and 30 spheres described the basal and apical trees, respectively. Age did not have significant effects in any of the Sholl spheres of the apical or basal dendrites (one-way ANOVA). (*D*) Examples of membrane potential recordings from Layer 3 PCs from neonatal and peripubertal monkeys. The subthreshold current injection ranged from −80 to 50 pA (500 ms steps). AP firing was evoked by injecting 400 pA (neonatal PC) and 450 pA (peripubertal PC). (*E*) Single action potentials recorded from a neonatal and peripubertal neuron superimposed. For additional information on intrinsic membrane properties, see Table 1.

from perisomatic synapses, as in developing PCs from rodent neocortex (Kobayashi et al. 2008; Lazarus and Huang 2011). To obtain an estimate of the developmental changes in IPSCs originating from perisomatic synapses, we evoked IPSCs by focal perisomatic extracellular stimulation (pIPSCs), using theta-glass stimulation electrodes placed near the soma. In PCs from rodent and monkey neocortex, pIPSCs have properties consistent with those originating from perisomatic GABA synapses (Kruglikov and Rudy 2008; Gonzalez-Burgos et al. 2009), suggesting that perisomatic stimulation predominantly activates GABAergic contacts at soma or proximal branches of the basal and apical dendrites (Somogyi et al. 1998). We elicited pIPSCs before and after applying ω-agatoxin IVA (agatoxin), a voltage-dependent calcium channel toxin that blocks GABA release from PV-positive but not from cholecystokinin (CCK)-positive perisomatic synapses (Hefft and Jonas 2005; Zaitsev et al. 2007; Kruglikov and Rudy 2008). In the rodent cortex pIPSCs display a prevalent agatoxin-sensitive component (Kruglikov and Rudy 2008). Therefore, we reasoned that if in monkey DLPFC Layer 3 PCs, perisomatic stimulation similarly elicits IPSCs predominantly via activation of perisomatic GABA synapses, then pIPSCs should have a large agatoxin-sensitive component (agaS-pIPSC). As shown in Figure 6*A*, the agaS-pIPSC accounted for ~80% of the total synaptic current in all age groups (neonatal: 81.5 ± 4.5%, prepubertal: 77.9 ± 3.9%, peripubertal: 79.21 ± 3.7%, adult:

Table 1
Intrinsic membrane properties of neonatal and peripubertal PCs

Parameter	Neonatal ($n = 8$)	Peripubertal ($n = 8$)	Student's t-test
Resting membrane potential (mV)	−71 ± 2	−70 ± 0.4	$t = 0.291$, $P = 0.775$
Input resistance (MΩ)	79.1 ± 9.9	71.0 ± 20.1	$t = 0.350$, $P = 0.732$
Membrane time constant (ms)	24.5 ± 1.4	22.6 ± 3.5	$t = 0.515$, $P = 0.616$
% Sag	91 ± 3	94 ± 6	$t = 0.280$, $P = 0.784$
Action potential threshold (mV)	−46 ± 3	−49 ± 1	$t = 0.999$, $P = 0.335$
Action potential duration (ms)	1.46 ± 0.06	1.30 ± 0.06	$t = 1.831$ $P = 0.088$
Action potential amplitude (mV)	81 ± 4	82 ± 4	$t = 0.091$, $P = 0.928$
Action potential overshoot (mV)	35 ± 4	32 ± 3	$t = 0.463$, $P = 0.650$
After hyperpolarization amplitude (mV)	10 ± 1	7.5 ± 1	$t = 2.07$, $P = 0.059$

Note: Data are shown as mean ± SEM. For details about the quantification of electrophysiological parameters, see Supplementary Methods.

82.9 ± 3.6; $F_{3,117} = 1.439$, $P = 0.235$), showing a nearly constant sensitivity to agatoxin between 1 and 64 months of age. The age-independent effects of agatoxin on pIPSCs suggest that the proportion of agatoxin-sensitive (putative PV-positive) versus agatoxin-resistant (putative CCK-positive) perisomatic inputs is stable with age. Our immunohistochemistry findings (Fig. 5) indicate that the densities of PV-positive or PV-negative perisomatic appositions do not change with age, but we did not directly assess CCK-positive perisomatic appositions. Interestingly, the constant agatoxin sensitivity suggests that the density of CCK-positive inputs remains constant as well, a prediction to be tested in future studies.

CCK-positive perisomatic synapses display endocannabinoid (eCB)-mediated depolarization-induced suppression of the IPSC (DSI) (Galarreta et al. 2008), but DSI is very weak or absent in distal CCK synapses (Lee et al. 2010). Thus, if as suggested previously (Kruglikov and Rudy 2008; Gonzalez-Burgos et al. 2009), perisomatic stimulation predominantly activates perisomatic GABAergic inputs, then the agatoxin-resistant pIPSC component (agaR-pIPSC) should display eCB-mediated DSI. We found that in 73% of the PCs tested, the agaR-pIPSCs displayed eCB-mediated DSI (Supplementary Fig. 2). Since DSI may significantly shape the activity of DLPFC PCs during cognitive tasks (Carter and Wang 2007), we compared the properties of DSI between age groups. However, neither the fraction of PCs with detectable DSI, the strength of DSI nor DSI duration differed between age groups (Supplementary Fig. 2*B,C*), suggesting that eCB modulation of synaptic inhibition has adult-like properties by early postnatal development. Using waveform subtraction, we separated the agaR-pIPSC, likely originated from eCB-sensitive CCK synapses, from the agaS-pIPSC, likely from PV synapses (Fig. 6*A*). We found that both the rise time and decay time constant of agaS-pIPSCs (Fig. 6*B*) and agaR-pIPSCs (Fig. 6*C*) shortened between neonatal and prepubertal age groups, suggesting significant age-related changes in IPSC duration at the 2 main populations of perisomatic GABA synapses.

At somatic vGAT/PV/γ2 appositions, presynaptic PV levels increased in the peripubertal age group (Fig. 5*G,H*). Interestingly, PV levels seem to positively correlate with the probability of GABA release (Pr) (Eggermann and Jonas 2012) and we found an age-related increase in mIPSC frequency (Fig. 4) that is consistent with an increase in Pr (Branco and Staras 2009). A higher Pr could explain the increase in mean sIPSC amplitude with age (Fig. 1*E*) observed in the absence of changes in mIPSC amplitude (Fig. 3*E*). Moreover, we found that agaS-pIPSCs displayed a form of short-term synaptic depression that increased with age (Supplementary Fig. 3*A*). However, contrary to the dogma established in glutamate synapses that changes in short-term depression are indicative of changes in Pr (Regehr 2012), in GABA synapses short-term depression is release-independent and insensitive to changes in Pr (Kraushaar and Jonas 2000; Hefft et al. 2002; Ma and Prince 2012). Interestingly, agatoxin, which decreases AP-evoked but not AP-independent GABA release (Goswami et al. 2012), had stronger effects on the amplitude of the larger sIPSCs recorded from peripubertal PCs (Supplementary Fig. 3*C*). These results suggest that the amplitude of sIPSCs originating from agatoxin-sensitive inputs (which include PV-positive perisomatic synapses) increases during development until the peripubertal period. However, further studies are necessary to determine the mechanisms underlying the age-related increase in IPSC amplitude and to determine whether IPSC amplitude increases with age at specific subtypes of agatoxin-sensitive inputs.

Developmental Changes in Synaptic Inhibition Enhance Gamma Oscillations in a Computational Model

We found significant developmental changes in IPSCs likely including those originated from PV-positive perisomatic inputs, which are essential for gamma oscillations (Buzsaki and Wang 2012). Therefore, we simulated activity in a model network to test the impact of the developmental changes in IPSCs on the capacity of DLPFC circuits to produce oscillations. Previous studies tested the effects of changing parameters of the inhibitory postsynaptic conductance (IPSG) in Interneuron-Network-Gamma (ING) models (Wang and Buzsaki 1996; White et al. 1998), and specifically in ING networks simulating hippocampal network development (Doischer et al. 2008). However, the effects of inhibitory synapses onto PCs cannot be studied using interneuron-only networks that do not include PCs (Doischer et al. 2008). Moreover, network synchrony is produced by markedly different mechanisms in ING versus Pyramidal-Interneuron-Network-Gamma (PING) models (Whittington et al. 2011) and current data favor PING over ING. For example, during the cycle of in vivo and in vitro gamma oscillations, as in PING, PCs fire first and interneuron firing follows a few milliseconds later, consistent with monosynaptic interneuron recruitment (Hajos and Paulsen 2009). In contrast, PC and interneuron firing is synchronous in ING (Borgers and Kopell 2003), and thus inconsistent with the empirical observations. Moreover, removing the inhibition critical for ING, via genetic ablation of $GABA_A$Rs selectively in PV-positive neurons, does not affect gamma oscillations (Wulff et al. 2009). In contrast, genetic deletion of AMPA receptors exclusively in PV cells, which removes the phasic excitation crucial for PING, markedly disrupts gamma (Fuchs et al. 2007).

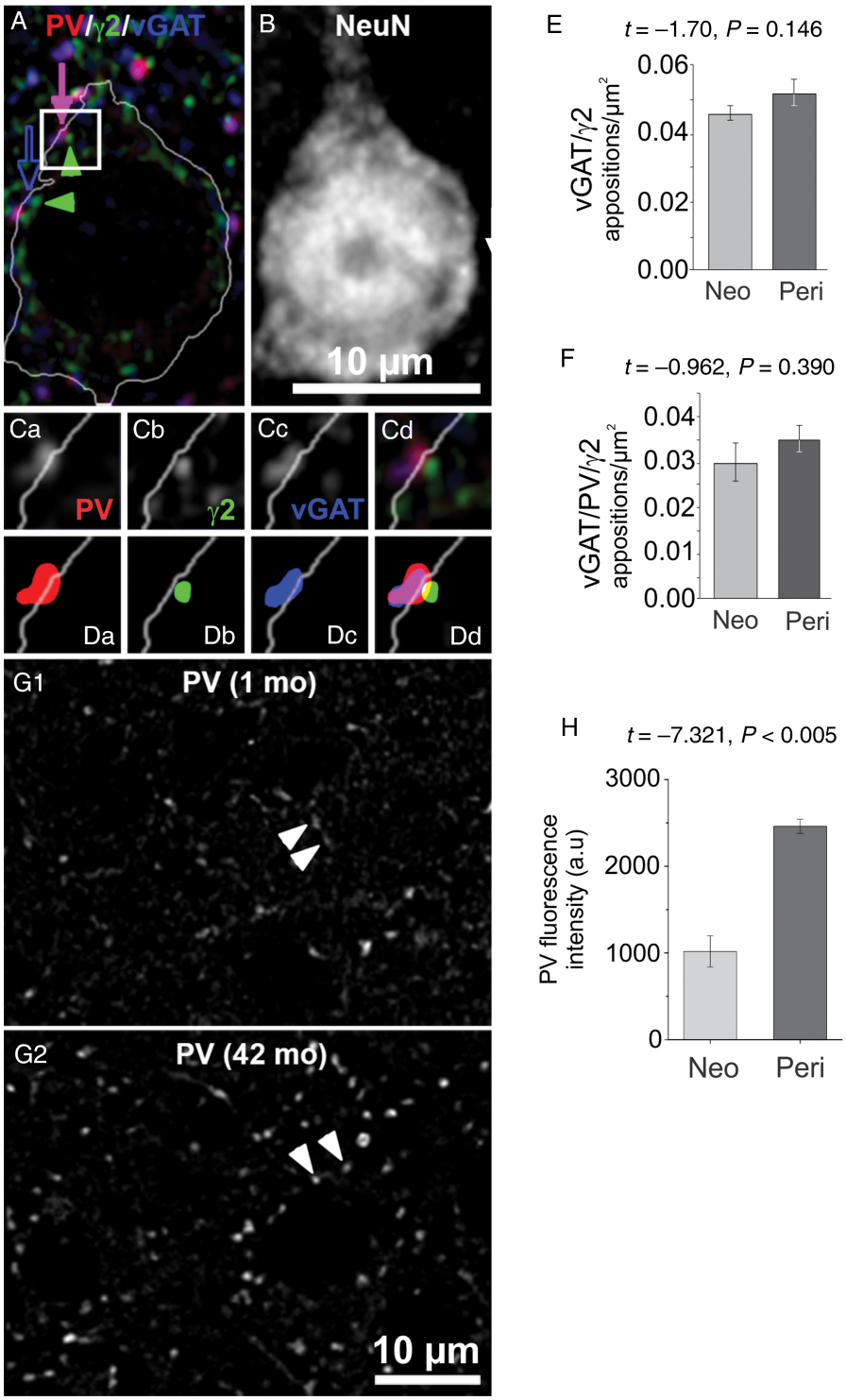

Figure 5. Somatic GABA synaptic appositions onto Layer 3 PCs. (*A*) Confocal image of a NeuN-positive PC (outline of the cell soma shown by a white line), PV-positive puncta (red), $GABA_AR$ gamma 2 subunit (γ2)-positive puncta (green) and vGAT-positive puncta (blue). A PV/vGAT/γ2 apposition is indicated by the solid arrow and green arrowhead. A vGAT/γ2 apposition is indicated by the open arrow and green arrowhead. The white outline of the soma was made using a mask object created by threshold segmentation of the NeuN signal (same field as in *B*). (*B*) Confocal image of NeuN signal of the field shown in *A*. The scale bar also applies to *A*. (*Ca–d*) 2× zoom view of the squared region in *A*. (*Da–d*) Object masks of the immunoreactive puncta in *Ca–d*. (*E*,*F*) Quantification of vGAT/γ2 (left) and vGAT/PV/γ2 (right) somatic apposition density. (*G*1,2) PV-positive puncta in tissue from neonatal and peripubertal monkeys. The arrows indicate PV-positive puncta that were identified as part of putative synaptic appositions onto the soma, using the vGAT and γ2 signal channels (not shown). (*H*) Quantification of PV mean fluorescence intensity in vGAT/PV/γ2 appositions.

We therefore built a model network of excitatory PCs (E cells) and inhibitory PV neurons (I cells) which, as in our previous study (Rotaru et al. 2011), generates oscillations via PING (Fig. 7*A*,*B*). We predicted that an increase in peak IPSG at I-to-E synapses (g_{ie}) may enhance gamma band synchrony only if the IPSG decay (τ_{ie}) shortens, as observed experimentally.

Otherwise, a larger IPSG may produce longer-lasting inhibition and limit substantially the production of oscillations with a period consistent with the gamma frequency band, as reported elsewhere (Volman et al. 2011). We modeled developmental change by leaving the number of inhibitory synapses constant, but varying g_{ie} from weak to strong and simultaneously shortening τ_{ie}. Oscillation frequency and power were measured for multiple combinations of g_{ie} and τ_{ie}, with all other parameters remaining constant.

Table 2

Mean protein levels, for presynaptic proteins vGAT and PV and postsynaptic γ2 per somatic GABAergic synaptic apposition in deep layer 3 PCs in DLPFC area 46

Protein	Neonatal mean fluorescence intensity (a.u.)	Peripubertal mean fluorescence intensity (a.u.)	Student's *t*-test
vGAT in vGAT/γ2 appositions	2608 ± 518	2099 ± 272	$t = 0.985$ $P = 0.380$
γ2 in vGAT/γ2 appositions	3655 ± 547	3650 ± 256	$t = 0.007$, $P = 0.990$
vGAT in vGAT/PV/γ2 appositions	2916 ± 530	2337 ± 168	$t = 1.042$, $P = 0.36$
γ2 in vGAT/PV/γ2 Appositions	3649 ± 512	3674 ± 245	$t = -0.044$, $P = 0.97$

Note: Data are shown as mean ± SEM. For details about quantification of protein levels in puncta, see Supplementary Methods.

Simulations in a network of 400 E cells and 80 I cells with sparse connectivity showed that as τ_{ie} increased without varying g_{ie}, the oscillation power decreased and the frequency was reduced. Reducing g_{ie} with constant τ_{ie} decreased oscillation power without substantial changes in frequency (Supplementary Fig. 4). To expand these findings by systematically exploring hundreds of parameter combinations (see Fig. 7*F*,*G* and Supplementary Figs 5 and 6), we used a smaller network (50 E cells and 20 I cells, see Materials and methods). As expected in PING, in a network with mature IPSG parameters, during the oscillation cycle I cells fired after E cells (Fig. 7*A*), maintaining a similar spike timing throughout multiple cycles (Fig. 7*B*). When g_{ie} was reduced and τ_{ie} prolonged to mimic the smaller size and slower decay kinetics of immature IPSCs, E and I cells fired with less temporal precision (Fig. 7*B*,*C*). To quantitatively assess rhythmic activity as a function of changes in g_{ie} and τ_{ie}, we determined the power spectral density of the synaptic gating variable s_e (Fig. 7*D*,*E*), which reflects population activity in the network model and the rhythmic variation of the membrane potential across the E cell population (Supplementary Fig. 4). Shortening τ_{ie} (from 20 to 1 ms) consistently increased the oscillation frequency (Fig. 7*F*). As inhibition increased from weak to strong (g_{ie} increasing from 0.2 to 2.2 mS/cm^2), the oscillation frequency decreased for a given value of τ_{ie}, and gamma band activity (frequency ≥30 Hz) was restricted to increasingly shorter τ_{ie} values (Fig. 7*F*). Analysis of

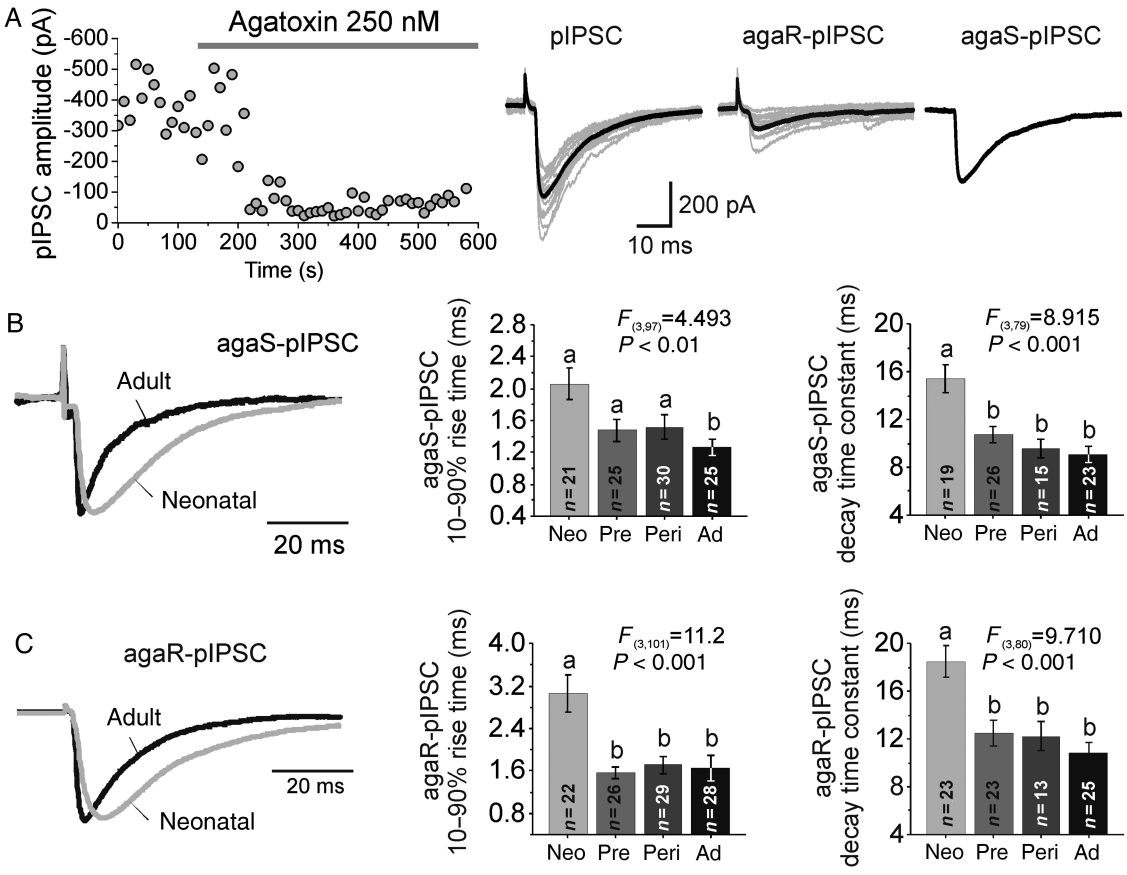

Figure 6. Age-related changes in perisomatic IPSC properties. (*A*) Left, time course of the effect of agatoxin on IPSCs evoked with perisomatic stimulation (pIPSCs). Right: representative recordings of pIPSCs (gray 10 consecutive traces, black, their average). The agatoxin-sensitive pIPSC (agaS-pIPSC) was obtained by subtracting the agatoxin-resistant pIPSC (agaR-pIPSC) from the total pIPSC. (*B*) Left, representative recordings of agaS-pIPSCs in PCs from neonatal and adult animals. pIPSC traces were normalized to the same amplitude. Middle, quantification of 10–90% rise time. Right, quantification of agaS-pIPSCs exponential decay time constant. (*C*) Same as in *B*, for agaR-pIPSCs.

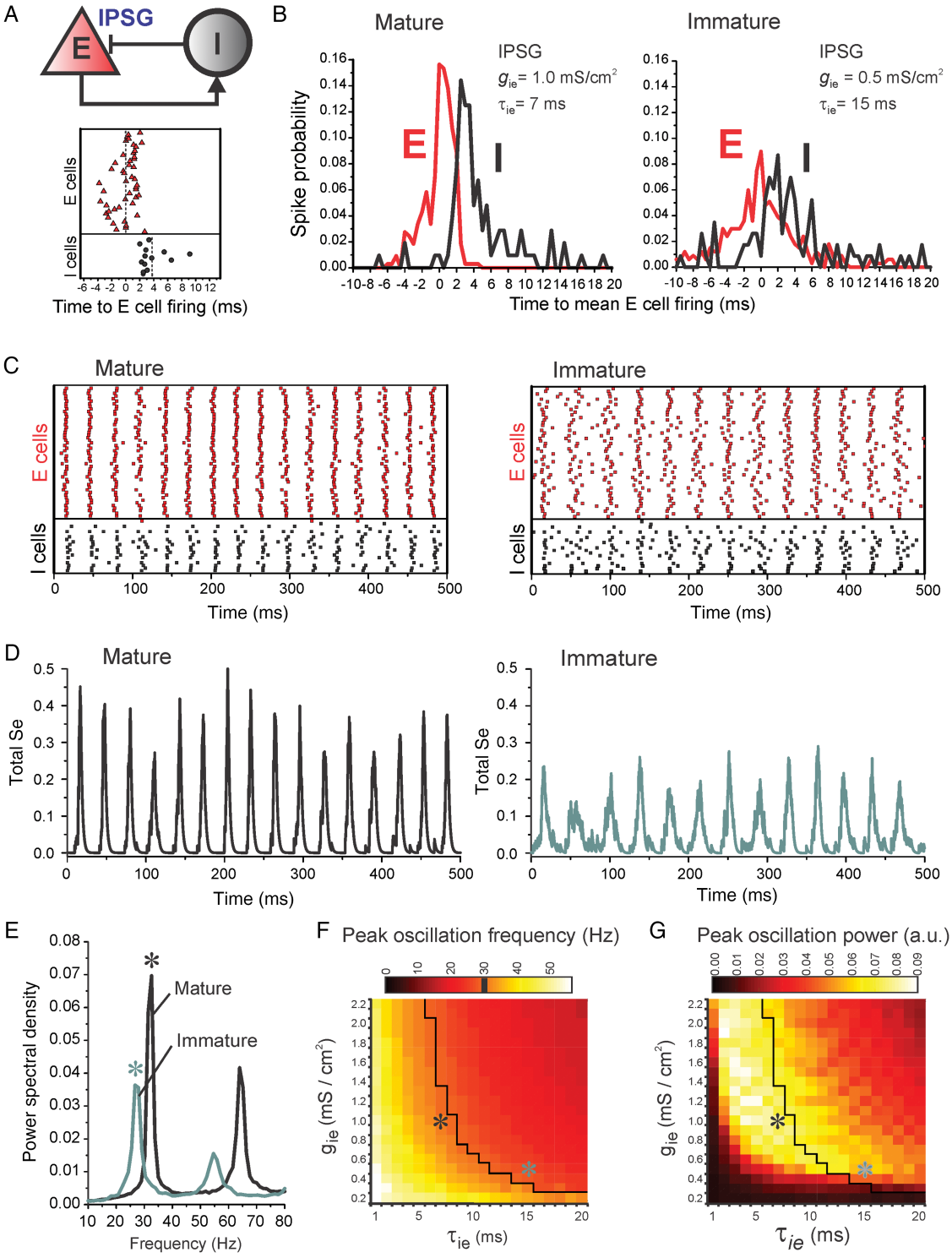

Figure 7. Effects of developmental changes in IPSCs on PING oscillations. (*A*) Top, scheme of recurrent connectivity among inhibitory (I) and excitatory (E) cells (I–I and E–E connections not shown). Bottom, spike timing of E and I cells relative to the mean time of E cell firing during a single oscillation cycle. Vertical dotted lines are the mean spike times for E and I cells. (*B*) Probability of E and I cell firing across the oscillation cycle, for mature (left) or immature (right) networks/IPSG parameters. (*C*) Spike raster plots for the E and I cells in mature (left) or immature (right) networks. (*D*) Plots of the synaptic gating variable s_e, which reflects population activity in the network model, versus time in mature (left) and immature (right) networks. (*E*) Power spectral density analysis of the synaptic gating variable s_e for mature (black) and immature (green) networks. Stars indicate the peak frequency and peak power values highlighted in *F* and *G*. (*F*) Peak oscillation frequency (in Hz) as a function of IPSG decay time constant (1–20 ms) and peak IPSG value (0.2–2.2 mS/cm^2). The black contour indicates the gamma band lower limit (30 Hz). (*G*) Peak oscillation power from the same simulations shown in *F*. Oscillation power is measured from the power spectral density plots (stars in *E*) for each combination of peak IPSG and IPSG decay time.

the oscillation power in the same set of simulations showed that when inhibition was weak (g_{ie} 0.2–0.4 mS/cm^2) oscillation power was very low (Fig. 7*G*). As g_{ie} increased, oscillation power increased consistently, although for longer τ_{ie} values the oscillation power decreased at higher g_{ie}. Therefore, significant gamma band power with stronger GABA synapses was

restricted to a relatively narrow range of short τ_{ie} values (Fig. 7*G*).

We found a small but statistically significant shortening of the IPSC exponential decay time between peripubertal and adult age groups (Fig. 1*D*). However, our simulations suggest that such a small change in decay time constant would have negligible effects on gamma band activity (Fig. 7*F*,*G*). We additionally tested the impact of 2 other factors. First, we varied the IPSG rise time between 0.1 and 2 ms, since the IPSC rise time shortened with age (Fig. 1*C*,*D*). However, we found that changes in IPSG rise time had very small effects on the oscillations (Supplementary Fig. 5). Second, we simulated the effects of changing the reversal potential for the $GABA_AR$ current (V_{in}) because whole-cell recording conditions alter V_{in} and performing perforated patch recordings to estimate V_{in} was not feasible in monkey DLPFC neurons. In rodent cortex, V_{in} turns hyperpolarizing during early postnatal development (Le Magueresse and Monyer 2013). Interestingly, in human DLPFC, mRNA levels for the chloride transporters KCC2 and NKCC1, the main regulators of V_{in} (Farrant and Kaila 2007), change before birth but are stable postnatally (Hyde et al. 2011). Using quantitative PCR and laser microdissection to collect RNA from individual Layer 3 PCs of monkey DLPFC, we found that the levels of KCC2 and NKCC1 mRNA were constant during postnatal development (Supplementary Fig. 6*A*). These data, together with previous studies (Hyde et al. 2011), suggest that in human and monkey DLPFC the hyperpolarizing shift in V_{in} occurs before birth. However, mRNA levels do not give information on protein expression, and, indeed, KCC2 protein levels in human neocortex increase during postnatal development (Dzhala et al. 2005). Thus, V_{in} may shift to hyperpolarizing values during a postnatal period when KCC2 mRNA expression is stable in primate DLPFC. Moreover, in addition to chloride transport across the membrane, local impermeant anions may be crucial for the polarity of the $GABA_AR$ current (Glykys et al. 2014). We therefore simulated the effects on oscillatory activity of varying V_{in}. We found that varying V_{in} below AP threshold (between −80 and −60 mV), thus keeping the IPSG effect inhibitory, only slightly affected network oscillations (Supplementary Fig. 6*B*). The effects of V_{in} values that determine a depolarizing shunting effect of the IPSG remain to be determined.

Discussion

In rodent cortex, inhibitory synaptogenesis and functional maturation of GABA synapses begin postnatally and follow similarly rapid trajectories, ending between postnatal weeks 3–4, well before adolescence (Le Magueresse and Monyer 2013). In primate neocortex, inhibitory synaptogenesis is completed before birth, but the expression of GABA synapse-related gene products changes significantly throughout postnatal development (Hoftman and Lewis 2011; Catts et al. 2013; Datta et al. 2015), suggesting that functional maturation of inhibitory synapses follows a protracted postnatal trajectory. Here, we used *in vitro* electrophysiology to assess for the first time the properties of $GABA_AR$-IPSCs during development of primate neocortex. We show that the maturation of GABA synapse function in monkey DLPFC layer 3 PCs is highly protracted relative to the time course of inhibitory synaptogenesis, with IPSCs changing significantly despite a constant mean density of inhibitory synapses across postnatal development (Bourgeois et al. 1994). We performed simulations in a computational network model and showed that, with stable inhibitory synapse density, the developmental changes in IPSC properties may have a significant impact on the production of oscillatory activity. Our experimental and modeling data suggest testable predictions for the postnatal trajectory of developmental changes in inhibition-based rhythms in primate DLPFC.

Limitations of This Study

GABA neurons exhibit highly diverse morphological, electrophysiological, and gene expression properties, suggesting a large number of GABA neuron subclasses is present in cortical circuits (Ascoli et al. 2008; DeFelipe et al. 2013). Interneuron diversity has been studied in greatest detail in the rodent hippocampus, where >20 subclasses were proposed to exist (Klausberger and Somogyi 2008). In Layer 3 of monkey DLPFC, up to date we characterized at least 9 subclasses of GABA neurons (Krimer et al. 2005; Zaitsev et al. 2005, 2009; Povysheva et al. 2007, 2008, 2013). However, a limitation of our current study is that we mainly assessed synaptic inhibition globally, via recordings of spontaneous IPSCs, and thus did not distinguish IPSCs generated by specific classes of GABA neurons. Recordings from synaptically connected cell pairs allow the study of inhibitory connections from identified GABA neurons and are feasible in the DLPFC of adult monkeys (Urban et al. 2002; Gonzalez-Burgos et al. 2004; Gonzalez-Burgos and Krimer et al. 2005). However, the cellular neurophysiology of immature GABA neurons is largely unexplored overall and has not been studied in the monkey DLPFC. Thus, connected cell pair experiments are unlikely to yield valuable information regarding GABA synapse development in monkey DLPFC before genetic labeling methods allow targeting for recording specific types of GABA neurons in the primate cortex, and in a manner independent of their maturation state. In some of the current experiments, we used focal extracellular stimulation applied near the PC soma, an approach previously shown to predominantly activate perisomatic GABA synapses (Kruglikov and Rudy 2008; Gonzalez-Burgos et al. 2009). The evoked IPSCs had several properties consistent with a perisomatic location of the GABA synapses involved, including fast rise time, strong sensitivity to agatoxin (consistent with activation of PV-positive perisomatic inputs) and significant endocannabinoid-mediated DSI (consistent with stimulation of CCK-positive perisomatic inputs). Thus, despite important limitations, our experiments revealed useful information regarding development of global synaptic inhibition and of agatoxin-sensitive IPSCs, which likely include those evoked by perisomatic PV-positive GABA synapses onto monkey DLPFC Layer 3 PCs.

Development of Synaptic Inhibition in Monkey DLPFC

Our present (Fig. 5) and previous (Fish et al. 2013) fluorescence microscopy data on GABA synaptic appositions are consistent with electron microscopy findings that in primate DLPFC the mean number of inhibitory synapses increases mainly prenatally and remains stable after birth (Bourgeois et al. 1994). The development of IPSC properties therefore shows that in monkey DLPFC the functional maturation of inhibition is temporally dissociated from developmental changes in inhibitory synapse number. These findings markedly contrast with those from rodent cortex, where inhibitory synaptogenesis (Micheva and Beaulieu 1996; De Felipe et al. 1997)

and functional maturation (Le Magueresse and Monyer 2013) follow very similar time courses, including a mainly postnatal onset.

Between the neonatal and prepubertal periods, the sIPSC amplitude in DLPFC PCs increased (Fig. 1*E*) but the mIPSC amplitude, which reflects the quantal response to GABA at single synaptic contacts or release sites (Auger and Marty 2000), was stable (Fig. 3*E*). We found that some sIPSCs in DLPFC neurons are AP-dependent. Since AP-dependent sIPSCs and AP-independent mIPSCs may derive from the same synaptic vesicle populations (Hua et al. 2010), the age-dependent increase in sIPSC amplitude may result from AP-dependent recruitment of a larger number of synapses or release sites, each producing a similar quantal response. Alternatively, sIPSCs and mIPSCs may originate from different synapse populations, such that the age-related increase in sIPSC amplitude reflects synapses with a larger quantal response to GABA. However, our quantitative fluorescence microscopy findings argue against the second possibility, because when vGAT/PV/γ2 or vGAT/γ2 synaptic appositions were assessed independent of contributing to sIPSCs or mIPSCs, the mean protein levels of vGAT (which may reflect the amount of GABA available for release) and γ2 (that may reflect the number of $GABA_A$Rs per synapse), did not change with age, consistent with a stable mIPSC size.

We found an age-related increase in the proportion of sIPSCs with both larger amplitude and shorter rise time, properties consistent with perisomatic inputs (Xiang et al. 2002; Lazarus and Huang 2011). However, the absence of change in the density of putative synaptic appositions onto the soma (Fig. 5) suggests a stable proportion of perisomatic synapses, even though many perisomatic synapses are found in proximal basal and apical dendrites and not the soma (Somogyi et al. 1998). Our experiments could not directly assess the mechanisms underlying the increase in the amplitude of sIPSCs (Fig. 1*E*) or agatoxin-sensitive sIPSCs (Supplementary Fig. 3). We found an increase in mIPSC frequency consistent with an age-related increase in GABA release probability and the agaSpIPSCs displayed an age-related increase in short-term depression. However, at GABA synapses short-term depression is release-independent and not correlated with release probability (Kraushaar and Jonas 2000; Hefft et al. 2002; Ma and Prince 2012). Therefore, in contrast to glutamate synapses, short-term depression cannot be used to reliably infer changes in release probability at GABA synapses. The mechanisms underlying the developmental increase in sIPSC amplitude with constant quantal response to GABA remain to be addressed.

Similarities and Differences with Development of Inhibition in Rodent Neocortex

Our study revealed that inhibitory synaptogenesis and functional maturation of GABA synapses in the primate DLPFC have temporally dissociated developmental trajectories, a finding in striking contrast to the development of rodent neocortex. However, we did find some remarkable similarities with prior studies of rodent neocortex. For example, the sIPSC decay time constant is essentially identical between layer 3 PCs in the DLPFC of adult monkeys versus medial prefrontal cortex of adult mice (Yoshino et al. 2011), and indistinguishable from that of unitary IPSCs elicited by single PV-positive basket cells in Layer 3 PCs of the prefrontal (Lazarus et al. 2015; Pafundo et al. 2013), somatosensory (Kobayashi et al. 2008) and visual (Lazarus and Huang 2011) cortices of adult mice. Since the IPSC decay time constant in PCs is crucial for gamma band oscillations (Fig. 7), the highly preserved value of IPSC decay may help explain the remarkably conserved properties of gamma rhythms across mammals and between cortical regions (Buzsaki et al. 2013).

The age-related shortening of IPSC decay time constant in layer 3 PCs of monkey DLPFC is similar to that previously found in cortical and hippocampal PCs in rodents. In rodents, developmental shortening of IPSC decay time is associated with an increased contribution from $GABA_A$Rs with α1 subunits (Le Magueresse and Monyer 2013), which deactivate 6 times faster than $GABA_A$Rs with other α subunits (Tia et al. 1996; Lavoie et al. 1997). Similar changes could underlie the decrease of IPSC decay time constant found here, since in monkey DLPFC the expression of $GABA_A$R α1 and α2 subunits increase and decrease with age, respectively, in total DLPFC tissue (Hashimoto et al. 2009), and specifically in Layer 3 PCs (Datta et al. 2015). $GABA_A$R channels containing α1 and α2 subunits have nearly identical single channel conductance (Lavoie et al. 1997) and we found that in Layer 3 PCs both γ2 subunit levels and mIPSC size were stable with age. Thus, one possibility is that an age-related switch from α1 to α2 subunits takes place in monkey DLPFC Layer 3 PCs with a constant number of $GABA_A$Rs per synapse, shortening the mIPSC decay while leaving mIPSC amplitude constant. We also found that, although the mIPSC size did not change, the sIPSC amplitude increased with age. A similar absence of developmental change in mIPSC amplitude, together with an increase in the amplitude of multisynaptic IPSCs was reported for developing PCs in rodents (Hollrigel and Soltesz 1997; Doischer et al. 2008; Kobayashi et al. 2008; Yang et al. 2013).

Current models of the pathophysiology of schizophrenia suggest that alterations in the development of synaptic inhibition (Hoftman and Lewis 2011; Catts et al. 2013), may lead to the deficits in neural oscillations and cognitive function in the disease (Gonzalez-Burgos et al. 2010). However, knowledge of the maturational processes that are altered in schizophrenia is very limited, in part because the normal development of synaptic inhibition is still poorly understood. Our data suggest that, while a useful and versatile system, the rodent cortex is a suboptimal model to study developmental processes relevant for schizophrenia. Although the IPSC strength increases and IPSC duration shortens with age in both monkeys and rodents, in primates such changes occur through a years-long postnatal period following stabilization of mean GABA synapse density, whereas in rodents the maturation of both inhibitory synapse number and function occur in parallel during the first 3–4 postnatal weeks. Since inhibitory synaptogenesis and functional maturation are prolonged and temporally dissociated in primates, but brief and nearly parallel in rodents, it is possible that the mechanisms underlying the developmental changes in IPSC properties differ across species. If so, not only the developmental time window of sensitivity to environmental and genetic factors, but also the effects that these factors may produce on IPSC development, could differ between primates and rodents.

Implications for the Developmental Trajectory of DLPFC Network Activity

Gamma oscillations in the DLPFC may be critical for cognition, and thus for cognitive development (Uhlhaas et al. 2010). The

power of the 40 Hz auditory steady-state response progressively increases with age, reaching a maximum by adolescence (Cho et al. 2015), whereas gamma band synchrony during a visual perception task increases between childhood, adolescence, and adulthood (Uhlhaas et al. 2010). However, neither the auditory steady-state response nor visual task-evoked activity are likely to reflect DLPFC circuit function or its development and the development of oscillatory activity in the primate DLPFC remains unexplored.

Here, we assessed the impact of developmental changes in IPSCs on DLPFC oscillations via simulations in a model network. We found that increasing g_{ie} while shortening τ_{ie}, to mimic IPSC development in Layer 3 PCs, increased oscillation frequency and power. Moreover, our data suggest specific predictions for the developmental trajectory of DLPFC oscillatory activity based on IPSC maturation. Particularly, since the IPSC decay shortened but the IPSC amplitude did not differ significantly between the neonatal and prepubertal periods, our results suggest that the frequency of inhibition-based rhythms increases during the neonatal-to-prepubertal transition, reaching the gamma band, but without a significant gain in power. Progressively after the prepubertal period, the increased IPSC strength may substantially boost gamma band power until adolescence, with the inhibition-based component of the oscillations remaining stable thereafter. Cognitive tasks elicit gamma band activity in local field potentials recorded extracellularly from various prefrontal cortical areas in adult monkeys (Buschman and Miller 2007; Gregoriou et al. 2009; Tsunada et al. 2011; Panagiotaropoulos et al. 2012). Moreover, cognitive tasks elicit an increase in gamma band synchrony in the frontal cortex of adult human subjects (Cho et al. 2006; Roux et al. 2012). However, the development of gamma oscillations in primate cortex has been studied only in human sensory and parietal cortical areas but not in the DLPFC. Therefore, the predictions derived from our results regarding gamma oscillation trajectory in primate DLPFC have to be tested in future studies.

Additional work is also necessary to test the impact of developmental changes in synaptic inhibition on nonrhythmic patterns of DLPFC network activity. For instance, stimulus-selective persistent neuronal firing in the adult DLPFC during working memory tasks critically depends on inhibitory control of NMDA receptor-dependent recurrent excitation between PCs (Wang et al. 2004, 2013). Some studies showed that persistent firing of single neurons in monkey DLPFC is temporally irregular and does not display robust rhythmicity (Compte et al. 2003). Interestingly, irregular activity of single neurons may contribute to population rhythms (Ardid et al. 2010), and thus to the increase in gamma oscillation power in the DLPFC during the delay of working memory tasks (Roux et al. 2012).

Cross-correlation analysis of spike trains recorded simultaneously from neuronal pairs in monkey DLPFC in vivo suggests that the strength of functional connectivity increases between peripubertal and postpubertal age, as a consequence of weaker inhibitory interactions (Zhou et al. 2014). However, we found that the strength of quantal $GABA_AR$-mediated transmission and the density of GABA synaptic appositions do not change with age, whereas $GABA_AR$-IPSCs evoked in layer 3 PCs had larger amplitude in peripubertal versus neonatal animals, but did not differ between peripubertal and postpubertal age groups. Our results therefore suggest that the reduced strength and prevalence of inhibitory interactions in the adult versus peripubertal DLPFC (Zhou et al. 2014) are not the direct consequence of a selective loss or weakening of $GABA_AR$-mediated inhibitory connections. Additional studies are necessary to determine if developmental changes in $GABA_BR$-mediated inhibition, which is prominent in Layer 3 PC dendrites in the DLPFC of adult monkeys (Gonzalez-Burgos et al. 2009), may contribute to the age-related increase in functional connectivity (Zhou et al. 2014). Moreover, in the DLPFC of adult monkeys, interneuron activity and GABA-mediated inhibition are tuned by neuromodulators such as dopamine (Gonzalez-Burgos et al. 2005; Kroner et al. 2007; Glausier et al. 2009; Jacob et al. 2013), and dopamine input to the monkey DLPFC shows a significantly protracted developmental change (Lewis 1997). However, it remains to be investigated whether dopamine or other neuromodulators of DLPFC activity change the effectiveness of GABA-mediated inhibition in an age-related manner.

Supplementary Material

Supplementary material can be found at: http://www.cercor.oxfordjournals.org/.

Funding

This work was supported by National Institutes of Health (grants MH051234, DA023109, MH096985, and MH084053) and National Science Foundation (grant DMS1219754).

Notes

We thank Ms Olga Krimer for excellent assistance with histochemical techniques and Neurolucida 3D reconstructions and Drs Nathaniel Urban, John Enwright, David Volk, and Raymond Cho for their useful comments. *Conflict of Interest:* D.A.L. currently receives investigator-initiated research support from Bristol-Myers Squibb and Pfizer and in 2012–2014 served as a consultant in the areas of target identification and validation and new compound development to Autifony, Bristol-Myers Squibb, Concert Pharmaceuticals, and Sunovion. A.R.S. is a consultant in statistical design to Janssen Pharmaceutical Research and Development, a Janssen Pharmaceutical Company.

References

Amatrudo JM, Weaver CM, Crimins JL, Hof PR, Rosene DL, Luebke JI. 2012. Influence of highly distinctive structural properties on the excitability of pyramidal neurons in monkey visual and prefrontal cortices. J Neurosci. 32:13644–13660.

Anderson SA, Classey JD, Conde F, Lund JS, Lewis DA. 1995. Synchronous development of pyramidal neuron dendritic spines and parvalbumin-immunoreactive chandelier neuron axon terminals in layer III of monkey prefrontal cortex. Neuroscience. 67:7–22.

Ardid S, Wang XJ, Gomez-Cabrero D, Compte A. 2010. Reconciling coherent oscillation with modulation of irregular spiking activity in selective attention: gamma-range synchronization between sensory and executive cortical areas. J Neurosci. 30:2856–2870.

Ascoli GA, Alonso-Nanclares L, Anderson SA, Barrionuevo G, Benavides-Piccione R, Burkhalter A, Buzsaki G, Cauli B, DeFelipe J, Fairen A et al. 2008. Petilla terminology: nomenclature of features of GABAergic interneurons of the cerebral cortex. Nat Rev Neurosci. 9:557–568.

Auger C, Marty A. 2000. Quantal currents at single-site central synapses. J Physiol. 526(Pt 1):3–11.

Borgers C, Kopell N. 2003. Synchronization in networks of excitatory and inhibitory neurons with sparse, random connectivity. Neural Comput. 15:509–538.

Bories C, Husson Z, Guitton MJ, De KY. 2013. Differential balance of prefrontal synaptic activity in successful versus unsuccessful cognitive aging. J Neurosci. 33:1344–1356.
Bourgeois JP, Goldman-Rakic PS, Rakic P. 1994. Synaptogenesis in the prefrontal cortex of rhesus monkeys. Cereb Cortex. 4:78–96.
Bourgeois JP, Rakic P. 1993. Changes of synaptic density in the primary visual cortex of the macaque monkey from fetal to adult stage. J Neurosci. 13:2801–2820.
Branco T, Staras K. 2009. The probability of neurotransmitter release: variability and feedback control at single synapses. Nat Rev Neurosci. 10:373–383.
Buschman TJ, Miller EK. 2007. Top-down versus bottom-up control of attention in the prefrontal and posterior parietal cortices. Science. 315:1860–1862.
Buzsaki G, Logothetis N, Singer W. 2013. Scaling brain size, keeping timing: evolutionary preservation of brain rhythms. Neuron. 80:751–764.
Buzsaki G, Wang XJ. 2012. Mechanisms of gamma oscillations. Annu Rev Neurosci. 35:203–225.
Carter E, Wang XJ. 2007. Cannabinoid-mediated disinhibition and working memory: dynamical interplay of multiple feedback mechanisms in a continuous attractor model of prefrontal cortex. Cereb Cortex. 17(Suppl 1):i16–i26.
Catts VS, Fung SJ, Long LE, Joshi D, Vercammen A, Allen KM, Fillman SG, Rothmond DA, Sinclair D, Tiwari Y et al. 2013. Rethinking schizophrenia in the context of normal neurodevelopment. Front Cell Neurosci. 7:60.
Chattopadhyaya B, Di CG, Higashiyama H, Knott GW, Kuhlman SJ, Welker E, Huang ZJ. 2004. Experience and activity-dependent maturation of perisomatic GABAergic innervation in primary visual cortex during a postnatal critical period. J Neurosci. 24:9598–9611.
Chaudhry FA, Reimer RJ, Bellocchio EE, Danbolt NC, Osen KK, Edwards RH, Storm-Mathisen J. 1998. The vesicular GABA transporter, VGAT, localizes to synaptic vesicles in sets of glycinergic as well as GABAergic neurons. J Neurosci. 18:9733–9750.
Cho RY, Konecky RO, Carter CS. 2006. Impairments in frontal cortical gamma synchrony and cognitive control in schizophrenia. Proc Natl Acad Sci USA. 103:19878–19883.
Cho RY, Walker CP, Polizzotto NR, Wozny TA, Fissell C, Chen CM, Lewis DA. 2015. Development of sensory gamma oscillations and cross-frequency coupling from childhood to early adulthood. Cereb Cortex. 25:1509–1518.
Compte A, Constantinidis C, Tegner J, Raghavachari S, Chafee MV, Goldman-Rakic PS, Wang XJ. 2003. Temporally irregular mnemonic persistent activity in prefrontal neurons of monkeys during a delayed response task. J Neurophysiol. 90:3441–3454.
Datta D, Arion D, Lewis DA. 2015. Developmental expression patterns of GABAA receptor subunits in layer 3 and 5 pyramidal cells of monkey prefrontal cortex. Cereb Cortex. 25:2295–2305.
DeFelipe J, Lopez-Cruz PL, Benavides-Piccione R, Bielza C, Larranaga P, Anderson S, Burkhalter A, Cauli B, Fairen A, Feldmeyer D et al. 2013. New insights into the classification and nomenclature of cortical GABAergic interneurons. Nat Rev Neurosci. 14:202–216.
De Felipe J, Marco P, Fairen A, Jones EG. 1997. Inhibitory synaptogenesis in mouse somatosensory cortex. Cereb Cortex. 7:619–634.
Doischer D, Hosp JA, Yanagawa Y, Obata K, Jonas P, Vida I, Bartos M. 2008. Postnatal differentiation of basket cells from slow to fast signaling devices. J Neurosci. 28:12956–12968.
Dzhala VI, Talos DM, Sdrula DA, Brumback AC, Mathews GC, Benke TA, Delpire E, Jensen FE, Staley K. 2005. NKCC1 transporter facilitates seizures in the developing brain. Nat Med. 11:1205–1213.
Eggermann E, Jonas P. 2012. How the 'slow' Ca(2+) buffer parvalbumin affects transmitter release in nanodomain-coupling regimes. Nat Neurosci. 15:20–22.
Etherington SJ, Williams SR. 2011. Postnatal development of intrinsic and synaptic properties transforms signaling in the layer 5 excitatory neural network of the visual cortex. J Neurosci. 31:9526–9537.
Farrant M, Kaila K. 2007. The cellular, molecular and ionic basis of GABA(A) receptor signalling. Prog Brain Res. 160:59–87.
Fish KN, Hoftman GD, Sheikh W, Kitchens M, Lewis DA. 2013. Parvalbumin-containing chandelier and basket cell boutons have distinctive modes of maturation in monkey prefrontal cortex. J Neurosci. 33:8352–8358.
Fritschy JM, Mohler H. 1995. GABAA-receptor heterogeneity in the adult rat brain: differential regional and cellular distribution of seven major subunits 88. J Comp Neurol. 359:154–194.
Fuchs EC, Zivkovic AR, Cunningham MO, Middleton S, LeBeau FE, Bannerman DM, Rozov A, Whittington MA, Traub RD, Rawlins JN et al. 2007. Recruitment of parvalbumin-positive interneurons determines hippocampal function and associated behavior. Neuron. 53:591–604.
Galarreta M, Erdelyi F, Szabo G, Hestrin S. 2008. Cannabinoid sensitivity and synaptic properties of 2 GABAergic networks in the neocortex. Cereb Cortex. 18:2296–2305.
Glausier JR, Khan ZU, Muly EC. 2009. Dopamine D1 and D5 receptors are localized to discrete populations of interneurons in primate prefrontal cortex. Cereb Cortex. 19:1820–1834.
Glykys J, Dzhala V, Egawa K, Balena T, Saponjian Y, Kuchibhotla KV, Bacskai BJ, Kahle KT, Zeuthen T, Staley KJ. 2014. Local impairment anions establish the neuronal chloride concentration. Science. 343:670–675.
Gogtay N, Giedd JN, Lusk L, Hayashi KM, Greenstein D, Vaituzis AC, Nugent TF III, Herman DH, Clasen LS, Toga AW et al. 2004. Dynamic mapping of human cortical development during childhood through early adulthood. Proc Natl Acad Sci USA. 101:8174–8179.
Gonzalez-Burgos G, Hashimoto T, Lewis DA. 2010. Alterations of cortical GABA neurons and network oscillations in schizophrenia. Curr Psychiatry Rep. 12:335–344.
Gonzalez-Burgos G, Krimer LS, Povysheva NV, Barrionuevo G, Lewis DA. 2005. Functional properties of fast spiking interneurons and their synaptic connections with pyramidal cells in primate dorsolateral prefrontal cortex. J Neurophysiol. 93:942–953.
Gonzalez-Burgos G, Krimer LS, Urban NN, Barrionuevo G, Lewis DA. 2004. Synaptic efficacy during repetitive activation of excitatory inputs in primate dorsolateral prefrontal cortex. Cereb Cortex. 14:530–542.
Gonzalez-Burgos G, Kroener S, Seamans JK, Lewis DA, Barrionuevo G. 2005. Dopaminergic modulation of short-term synaptic plasticity in fast-spiking interneurons of primate dorsolateral prefrontal cortex. J Neurophysiol. 94:4168–4177.
Gonzalez-Burgos G, Kroener S, Zaitsev AV, Povysheva NV, Krimer LS, Barrionuevo G, Lewis DA. 2008. Functional maturation of excitatory synapses in layer 3 pyramidal neurons during postnatal development of the primate prefrontal cortex. Cereb Cortex. 18:626–637.
Gonzalez-Burgos G, Rotaru DC, Zaitsev AV, Povysheva NV, Lewis DA. 2009. GABA transporter GAT1 prevents spillover at proximal and distal GABA synapses onto primate prefrontal cortex neurons. J Neurophysiol. 101:533–547.
Goswami SP, Bucurenciu I, Jonas P. 2012. Miniature IPSCs in hippocampal granule cells are triggered by voltage-gated Ca2+ channels via microdomain coupling. J Neurosci. 32:14294–14304.
Gregoriou GG, Gotts SJ, Zhou H, Desimone R. 2009. Long-range neural coupling through synchronization with attention. Prog Brain Res. 176:35–45.
Guo C, Stella SL Jr, Hirano AA, Brecha NC. 2009. Plasmalemmal and vesicular gamma-aminobutyric acid transporter expression in the developing mouse retina. J Comp Neurol. 512:6–26.
Hajos N, Paulsen O. 2009. Network mechanisms of gamma oscillations in the CA3 region of the hippocampus. Neural Netw. 22:1113–1119.
Hashimoto T, Nguyen QL, Rotaru D, Keenan T, Arion D, Beneyto M, Gonzalez-Burgos G, Lewis DA. 2009. Protracted developmental trajectories of GABAA receptor alpha1 and alpha2 subunit expression in primate prefrontal cortex. Biol Psychiatry. 65: 1015–1023.
Hefft S, Jonas P. 2005. Asynchronous GABA release generates long-lasting inhibition at a hippocampal interneuron-principal neuron synapse. Nat Neurosci. 8:1319–1328.
Hefft S, Kraushaar U, Geiger JR, Jonas P. 2002. Presynaptic short-term depression is maintained during regulation of transmitter release at a GABAergic synapse in rat hippocampus. J Physiol. 539:201–208.
Hensch TK. 2005. Critical period plasticity in local cortical circuits. Nat Rev Neurosci. 6:877–888.

Henze DA, Gonzalez-Burgos GR, Urban NN, Lewis DA, Barrionuevo G. 2000. Dopamine increases excitability of pyramidal neurons in primate prefrontal cortex. J Neurophysiol. 84:2799–2809.
Hoftman GD, Lewis DA. 2011. Postnatal developmental trajectories of neural circuits in the primate prefrontal cortex: identifying sensitive periods for vulnerability to schizophrenia. Schizophr Bull. 37:493–503.
Hollrigel GS, Soltesz I. 1997. Slow kinetics of miniature IPSCs during early postnatal development in granule cells of the dentate gyrus. J Neurosci. 17:5119–5128.
Hua Y, Sinha R, Martineau M, Kahms M, Klingauf J. 2010. A common origin of synaptic vesicles undergoing evoked and spontaneous fusion. Nat Neurosci. 13:1451–1453.
Hyde TM, Lipska BK, Ali T, Mathew SV, Law AJ, Metitiri OE, Straub RE, Ye T, Colantuoni C, Herman MM et al. 2011. Expression of GABA signaling molecules KCC2, NKCC1, and GAD1 in cortical development and schizophrenia. J Neurosci. 31:11088–11095.
Izhikevich EM. 2004. Which model to use for cortical spiking neurons? IEEE Trans Neural Netw. 15:1063–1070.
Jacob SN, Ott T, Nieder A. 2013. Dopamine regulates two classes of primate prefrontal neurons that represent sensory signals. J Neurosci. 33:13724–13734.
Kagi U, Berchtold MW, Heizmann CW. 1987. Ca2+-binding parvalbumin in rat testis. Characterization, localization, and expression during development. J Biol Chem. 262:7314–7320.
Khazipov R, Minlebaev M, Valeeva G. 2013. Early gamma oscillations. Neuroscience. 250:240–252.
Klausberger T, Somogyi P. 2008. Neuronal diversity and temporal dynamics: the unity of hippocampal circuit operations. Science. 321:53–57.
Kobayashi M, Hamada T, Kogo M, Yanagawa Y, Obata K, Kang Y. 2008. Developmental profile of GABAA-mediated synaptic transmission in pyramidal cells of the somatosensory cortex. Eur J Neurosci. 28: 849–861.
Kraushaar U, Jonas P. 2000. Efficacy and stability of quantal GABA release at a hippocampal interneuron-principal neuron synapse. J Neurosci. 20:5594–5607.
Krimer LS, Zaitsev AV, Czanner G, Kroner S, Gonzalez-Burgos G, Povysheva NV, Iyengar S, Barrionuevo G, Lewis DA. 2005. Cluster analysis-based physiological classification and morphological properties of inhibitory neurons in layers 2–3 of monkey dorsolateral prefrontal cortex. J Neurophysiol. 94:3009–3022.
Kroner S, Krimer LS, Lewis DA, Barrionuevo G. 2007. Dopamine increases inhibition in the monkey dorsolateral prefrontal cortex through cell type-specific modulation of interneurons. Cereb Cortex. 17:1020–1032.
Kruglikov I, Rudy B. 2008. Perisomatic GABA release and thalamocortical integration onto neocortical excitatory cells are regulated by neuromodulators. Neuron. 58:911–924.
Lavoie AM, Tingey JJ, Harrison NL, Pritchett DB, Twyman RE. 1997. Activation and deactivation rates of recombinant GABA(A) receptor channels are dependent on alpha-subunit isoform. Biophys J. 73:2518–2526.
Lazarus MS, Huang ZJ. 2011. Distinct maturation profiles of perisomatic and dendritic targeting GABAergic interneurons in the mouse primary visual cortex during the critical period of ocular dominance plasticity. J Neurophysiol. 106:775–787.
Lazarus MS, Krishnan K, Huang ZJ. 2015. GAD67 Deficiency in parvalbumin interneurons produces deficits in inhibitory transmission and network disinhibition in mouse prefrontal cortex. Cereb Cortex. 25:1290–1296.
Lee SH, Foldy C, Soltesz I. 2010. Distinct endocannabinoid control of GABA release at perisomatic and dendritic synapses in the hippocampus. J Neurosci. 30:7993–8000.
Le Magueresse C, Monyer H. 2013. GABAergic Interneurons shape the functional maturation of the cortex. Neuron. 77:388–405.
Lewis DA. 1997. Development of the prefrontal cortex during adolescence: insights into vulnerable neural circuits in schizophrenia. Neuropsychopharmacology. 16:385–398.
Ma Y, Prince DA. 2012. Functional alterations in GABAergic fast-spiking interneurons in chronically injured epileptogenic neocortex. Neurobiol Dis. 47:102–113.
Maffei A, Lambo ME, Turrigiano GG. 2010. Critical period for inhibitory plasticity in rodent binocular V1. J Neurosci. 30:3304–3309.
Micheva KD, Beaulieu C. 1996. Quantitative aspects of synaptogenesis in the rat barrel field cortex with special reference to GABA circuitry. J Comp Neurol. 373:340–354.
Mullen RJ, Buck CR, Smith AM. 1992. NeuN, a neuronal specific nuclear protein in vertebrates. Development. 116:201–211.
Pafundo DE, Miyamae T, Lewis DA, Gonzalez-Burgos G. 2013. Cholinergic modulation of neuronal excitability and recurrent excitation-inhibition in prefrontal cortex circuits: implications for gamma oscillations. J Physiol. 591:4725–4728.
Panagiotaropoulos TI, Deco G, Kapoor V, Logothetis NK. 2012. Neuronal discharges and gamma oscillations explicitly reflect visual consciousness in the lateral prefrontal cortex. Neuron. 74:924–935.
Plant TM. 1988. Neuroendocrine basis of puberty in the rhesus monkey (*Macaca mulatta*). Front Neuroendocrinol. 10:215–238.
Povysheva NV, Zaitsev AV, Gonzalez-Burgos G, Lewis DA. 2013. Electrophysiological heterogeneity of fast-spiking interneurons: chandelier versus basket cells. PLoS One. 8:e70553.
Povysheva NV, Zaitsev AV, Kroener S, Krimer OA, Rotaru DC, Gonzalez-Burgos G, Lewis DA, Krimer LS. 2007. Electrophysiological Differences between Neurogliaform Cells from Monkey and Rat Prefrontal Cortex. J Neurophysiol. 97:1030–1039.
Povysheva NV, Zaitsev AV, Rotaru DC, Gonzalez-Burgos G, Lewis DA, Krimer LS. 2008. Parvalbumin-positive basket interneurons in monkey and rat prefrontal cortex. J Neurophysiol. 100:2348–2360.
Preuss TM. 1995. Do rats have prefrontal cortex? The Rose–Woolsey–Akert program reconsidered. J Cogn Neurosci. 7:1–24.
Regehr WG. 2012. Short-term presynaptic plasticity. Cold Spring Harb Perspect Biol. 4:a005702.
Ridler TW, Calvard S. 1978. Picture thresholding using an iterative selection method. IEEE Trans Systems Man Cybern. 8:630–632.
Rotaru DC, Yoshino H, Lewis DA, Ermentrout GB, Gonzalez-Burgos G. 2011. Glutamate receptor subtypes mediating synaptic activation of prefrontal cortex neurons: relevance for schizophrenia. J Neurosci. 31:142–156.
Roux F, Wibral M, Mohr HM, Singer W, Uhlhaas PJ. 2012. Gamma-band activity in human prefrontal cortex codes for the number of relevant items maintained in working memory. J Neurosci. 32:12411–12420.
Somogyi P, Tamas G, Lujan R, Buhl EH. 1998. Salient features of synaptic organisation in the cerebral cortex. Brain Res Rev. 26:113–135.
Stuart G, Spruston N. 1998. Determinants of voltage attenuation in neocortical pyramidal neuron dendrites. J Neurosci. 18:3501–3510.
Tia S, Wang JF, Kotchabhakdi N, Vicini S. 1996. Distinct deactivation and desensitization kinetics of recombinant GABAA receptors. Neuropharmacology. 35:1375–1382.
Tsunada J, Baker AE, Christison-Lagay KL, Davis SJ, Cohen YE. 2011. Modulation of cross-frequency coupling by novel and repeated stimuli in the primate ventrolateral prefrontal cortex. Front Psychol. 2:217.
Uhlhaas PJ, Roux F, Rodriguez E, Rotarska-Jagiela A, Singer W. 2010. Neural synchrony and the development of cortical networks. Trends Cogn Sci. 14:72–80.
Urban NN, Gonzalez-Burgos G, Henze DA, Lewis DA, Barrionuevo G. 2002. Selective reduction by dopamine of excitatory synaptic inputs to pyramidal neurons in primate prefrontal cortex. J Physiol. 539:707–712.
Volman V, Behrens MM, Sejnowski TJ. 2011. Downregulation of parvalbumin at cortical GABA synapses reduces network gamma oscillatory activity. J Neurosci. 31:18137–18148.
Wang M, Yang Y, Wang CJ, Gamo NJ, Jin LE, Mazer JA, Morrison JH, Wang XJ, Arnsten AF. 2013. NMDA receptors subserve persistent neuronal firing during working memory in dorsolateral prefrontal cortex. Neuron. 77:736–749.
Wang XJ, Buzsaki G. 1996. Gamma oscillation by synaptic inhibition in a hippocampal interneuronal network model. J Neurosci. 16:6402–6413.
Wang XJ, Tegner J, Constantinidis C, Goldman-Rakic PS. 2004. Division of labor among distinct subtypes of inhibitory neurons in a cortical microcircuit of working memory. Proc Natl Acad Sci USA. 101:1368–1373.
White JA, Chow CC, Ritt J, Soto-Trevino C, Kopell N. 1998. Synchronization and oscillatory dynamics in heterogeneous, mutually inhibited neurons. J Comput Neurosci. 5:5–16.

Whittington MA, Cunningham MO, LeBeau FE, Racca C, Traub RD. 2011. Multiple origins of the cortical gamma rhythm. Dev Neurobiol. 71:92–106.

Williams SR, Mitchell SJ. 2008. Direct measurement of somatic voltage clamp errors in central neurons. Nat Neurosci. 11:790–798.

Workman AD, Charvet CJ, Clancy B, Darlington RB, Finlay BL. 2013. Modeling transformations of neurodevelopmental sequences across mammalian species. J Neurosci. 33:7368–7383.

Wulff P, Ponomarenko AA, Bartos M, Korotkova TM, Fuchs EC, Bahner F, Both M, Tort AB, Kopell NJ, Wisden W et al. 2009. Hippocampal theta rhythm and its coupling with gamma oscillations require fast inhibition onto parvalbumin-positive interneurons. Proc Natl Acad Sci USA. 106:3561–3566.

Xiang Z, Huguenard JR, Prince DA. 2002. Synaptic inhibition of pyramidal cells evoked by different interneuronal subtypes in layer v of rat visual cortex. J Neurophysiol. 88:740–750.

Yang JM, Zhang J, Yu YQ, Duan S, Li XM. 2013. Postnatal development of 2 microcircuits involving fast-spiking interneurons in the mouse prefrontal cortex. Cereb Cortex. 24:98–109.

Yoshino H, Miyamae T, Hansen G, Zambrowicz B, Flynn M, Pedicord D, Blat Y, Westphal RS, Zaczek R, Lewis DA et al. 2011. Postsynaptic diacylglycerol lipase mediates retrograde endocannabinoid suppression of inhibition in mouse prefrontal cortex. J Physiol. 589:4857–4884.

Zaitsev AV, Gonzalez-Burgos G, Povysheva NV, Kroner S, Lewis DA, Krimer LS. 2005. Localization of calcium-binding proteins in physiologically and morphologically characterized interneurons of monkey dorsolateral prefrontal cortex. Cereb Cortex. 15:1178–1186.

Zaitsev AV, Povysheva NV, Gonzalez-Burgos G, Lewis DA. 2012. Electrophysiological classes of layer 2/3 pyramidal cells in monkey prefrontal cortex. J Neurophysiol. 108:595–609.

Zaitsev AV, Povysheva NV, Gonzalez-Burgos G, Rotaru D, Fish KN, Krimer LS, Lewis DA. 2009. Interneuron diversity in layers 2–3 of monkey prefrontal cortex. Cereb Cortex. 19:1597–1615.

Zaitsev AV, Povysheva NV, Lewis DA, Krimer LS. 2007. P/Q-type, but not N-type, calcium channels mediate GABA release from fast-spiking interneurons to pyramidal cells in rat prefrontal cortex. J Neurophysiol. 97:3567–3573.

Zhang ZW. 2004. Maturation of layer V pyramidal neurons in the rat prefrontal cortex: intrinsic properties and synaptic function. J Neurophysiol. 91:1171–1182.

Zhou X, Zhu D, Katsuki F, Qi XL, Lees CJ, Bennett AJ, Salinas E, Stanford TR, Constantinidis C. 2014. Age-dependent changes in prefrontal intrinsic connectivity. Proc Natl Acad Sci USA. 111:3853–3858.

Zhu JJ. 2000. Maturation of layer 5 neocortical pyramidal neurons: amplifying salient layer 1 and layer 4 inputs by Ca2+ action potentials in adult rat tuft dendrites. J Physiol. 526(Pt 3):571–587.